ROYAL SOCIETY
OF CHEMISTRY

FOCUS

Check for updates

Organic building blocks at inorganic nanomaterial interfaces

Yunping Huang, [iD] [a] Theodore A. Cohen, [iD] [b] Breena M. Sperry, [a] Helen Larson, [c] Hao A. Nguyen, [c] Micaela K. Homer, [iD] [c] Florence Y. Dou, [iD] [c] Laura M. Jacoby, [iD] [c] Brandi M. Cossairt, [c] Daniel R. Gamelin [iD] [c] and Christine K. Luscombe [iD] †*[abc]

This tutorial review presents our perspective on designing organic molecules for the functionalization of inorganic nanomaterial surfaces, through the model of an "anchor-functionality" paradigm. This "anchor-functionality" paradigm is a streamlined design strategy developed from a comprehensive range of materials (*e.g.*, lead halide perovskites, II–VI semiconductors, III–V semiconductors, metal oxides, diamonds, carbon dots, silicon, *etc.*) and applications (*e.g.*, light-emitting diodes, photovoltaics, lasers, photonic cavities, photocatalysis, fluorescence imaging, photo dynamic therapy, drug delivery, *etc.*). The structure of this organic interface modifier comprises two key components: anchor groups binding to inorganic surfaces and functional groups that optimize their performance in specific applications. To help readers better understand and utilize this approach, the roles of different anchor groups and different functional groups are discussed and explained through their interactions with inorganic materials and external environments.

1. Introduction

Inorganic nanomaterials possess unique physical, chemical, electronic, and optical properties different from their bulk counterparts. Such properties stem from their high surface areas and from quantum confinement effects,[1–7] opening new opportunities for innovative technology concepts. For example, the high efficiency and narrow emission of quantum dots (QDs) promote energy efficiency and color quality in TV and cell phone displays, attracting significant attention in the commercial market.[8,9] Meanwhile, many other technologies based on inorganic nanomaterials are currently undergoing rapid development towards future commercialization, covering both conventional semiconductor domains (*e.g.*, solar cells[10,11] and light-emitting diodes[12–15]) and newly emergent technology concepts (*e.g.*, photocatalysis,[16,17] nanomedicine,[18,19] spintronics[20–22] and quantum computing[23,24]).

With at least one external dimension reduced to below 100 nm, the surface area to volume ratios of nanomaterials are larger than those of bulk materials by orders of magnitude. Additionally, these terminal surfaces tend to form chemical

bonds with or otherwise absorb nearby molecules to reach a thermodynamically stable state. Depending on the size of the incoming molecules, the interfacial layer thickness can be as small as ~ 0.1 nm in the case of H-terminated diamonds or oxides, or as large as ~ 2 nm when polymers are adsorbed onto a QD surface.[25] Thin as they are, such alteration of the surface can induce dramatic changes to the material's properties. For example, a hydrogen mono-layer on the surface of diamond thin films induces band bending extending as deep as 150 nm below the interface,[26] and subsequently a $\sim 10^5$ increase in conductivity.[27–29] Similar electronic effects are observed in QDs as well, although now with the crystal's physical dimensions often smaller than the depletion widths. For example, surface dipoles generated by mono-layers of organic molecules on QD surfaces can tune band-edge potentials of PbS QDs by over 1 eV.[30,31] The effects of interface engineering are not limited to the manipulation of electronic structures, but also dispersity, molecular interaction, and the stability of the nanomaterials, which will be discussed in the following sections. These examples highlight the efficacy of interface engineering as an attractive complement to conventional methods such as composition and phase engineering to regulate the properties of inorganic nanomaterials.

Controlled-atmosphere annealing and plasma treatment are common conventional methods for the modification of inorganic surfaces. However, these methods give rather limited choices for surface functionalization, terminating the material surface with hydrogen, oxygen, nitrogen, or chlorine atoms.[32]

[a] Department of Materials Science & Engineering, University of Washington, Seattle, WA 98195, USA. E-mail: christine.luscombe@oist.jp

[b] Molecular Engineering & Sciences Institute, University of Washington, Seattle, WA 98195, USA

[c] Department of Chemistry, University of Washington, Seattle, WA 98195, USA

† Current address: Pi-Conjugated Polymers Unit, Okinawa Institute of Science & Technology Graduate University, Onna-son, Okinawa, Japan.

Fortunately, this limitation has been alleviated by the collaborative efforts from both inorganic and organic chemists in the past decade. Taking advantage of the structural flexibility and tunability of organic compounds, a variety of organic molecules were introduced to the surfaces of inorganic and related nanomaterials, showing great potential for different material types (e.g., lead-halide perovskites, II–VI semiconductors, III–V semiconductors, metal oxides, diamond, carbon dots, silicon, etc.), and for different applications (e.g., light-emitting diodes (LEDs), photovoltaics (PVs), lasers, photonic cavities, photocatalysis, fluorescent imaging, photodynamic therapy, drug delivery, etc.). Several reviews have comprehensively summarized these surface modification methods regarding one or several specific types of materials or applications.[32–35] On the other hand, research in inorganic nanomaterials is quickly evolving, with new materials being developed and applications expanding. To guide and facilitate developments of emerging materials and applications, it is crucial to generalize the principles of interface engineering by summarizing a wide scope of previous examples in both material types and applications.

In this tutorial review, we share a generalized molecular paradigm for organic molecules used for interface modification of inorganic nanomaterials - the "anchor-functionality" design shown in Fig. 1. The anchor group is a building block that binds to nanomaterial surfaces, either through ionic or covalent bonding depending on the target nanomaterial; the functional group is a building block that endows the nanomaterials with targeted functionalities to cater to different requirements depending on the different applications. Once the anchor group and the functional group are selected, a linker (usually inert alkyl chains or polymer backbones) covalently attaches the anchor group and the functional group. The linker, anchor, and functional groups together constitute an interface modifier. The interaction between anchor groups and different types of inorganic materials will be discussed in Section 2. In Section 3, we discuss the mechanism by which functional groups endow new functionalities to nanomaterials. Considering this field is a highly interdisciplinary field with researchers from different backgrounds (including organic chemists, inorganic chemists, physicists, healthcare professionals), the "anchor-functionality" paradigm offers researchers with a non-chemistry background an accessible toolset to understand interface molecules. We hope that this will help bridge the knowledge gap between researchers and facilitate in-depth discussion for future interdisciplinary collaborations, expediting solutions to current challenges leading to future innovations.

2. Anchor groups for different interfaces

The binding modes, affinities, and types of capping ligands that can be bound to the surfaces of nanomaterials depend on the nature of the ligand-surface interactions. Nanocrystals (NCs) can be broadly categorized in terms of their lattice ionicity, which spans from purely covalent (diamond) to highly ionic (metal-halide perovskites), and this ionicity frequently dictates the nature of the interface. Such a variety of lattice features requires matching to different anchor groups to form a molecular interaction between ligands and their target nanomaterials. Therefore, in Section 2, we highlight the common inorganic nanomaterial surfaces and explain their interactions with different anchor groups, to elucidate the "anchor" component in the "anchor-functionality" design.

The synthesis and processing of metal-halide perovskite NCs is a good example to illustrate the anchor group interactions at the surface of an ionic lattice. Oleylammonium is often used as a ligand to stabilize perovskite NCs and to prevent large aggregate formation during grain growth.[36] In this case, the ammonium group is the anchor group of the ligand attaching to the surfaces of the NCs. Due to the high ionicity of the perovskite lattice, the ammonium groups desorb and reattach to the perovskite surface in a dynamic equilibrium, which allows the precursor ions (e.g., Pb^{2+}, Cs^+, I^-) to freely move into the lattice and grow the NC core structure. Moreover, this ionic interaction allows facile ligand exchange after NC synthesis, offering a convenient method to further tailor the NC properties.

When an ionic core is shelled by a more covalent lattice, the ionic core is shielded, and ligand exchange is inhibited. For example, the core of CdSe QDs will no longer be able to react once the surface is terminated with a silica shell. On the other hand, such strong covalent bonds provide excellent isolation that shields the CdSe core from external molecules, and thus silica shelling is a common method used to enhance the stability of QDs.

In the following sections, we discuss examples of anchor-surface interactions based on these two different lattice types. In the ionic lattice section (Section 2.1), we discuss II–VI semiconductors, III–V semiconductors, metal oxides, I–III–VI nanoparticles, and lead halide perovskites. The covalent lattice surface section (Section 2.2) discusses surface binding for diamond, silicon, and silica. Although we are not able to include all material types, we believe the above examples are sufficient to explain the interactions between anchors and nanomaterials and demonstrate the wide application scope of this "anchor-functionality" paradigm.

2.1 Anchor groups for surfaces of ionic lattices

2.1.1 II–VI QDs, III–V QDs, metal oxides, I–III–VI nanocrystals. In 1981 and 1983, the quantum size effect was demonstrated for CuCl[4] and CdS[5] NCs. Since then, II–VI QDs, III–V QDs, metal oxide NCs, and I–III–VI NCs have attracted broad research interest. Although they possess differences in composition, they share similar interactions with anchor groups and have related bandgap-modifying size effects.[32,37] Stoichiometric or neutral nanomaterial surfaces are stabilized by neutral ligands, whereas non-stoichiometric surface compositions require charge balance from charged ligands.[38] Applying the covalent bond classification scheme to the interactions between the ligand anchor group and NC surface site gives three limiting ligand types as follows: the L-type
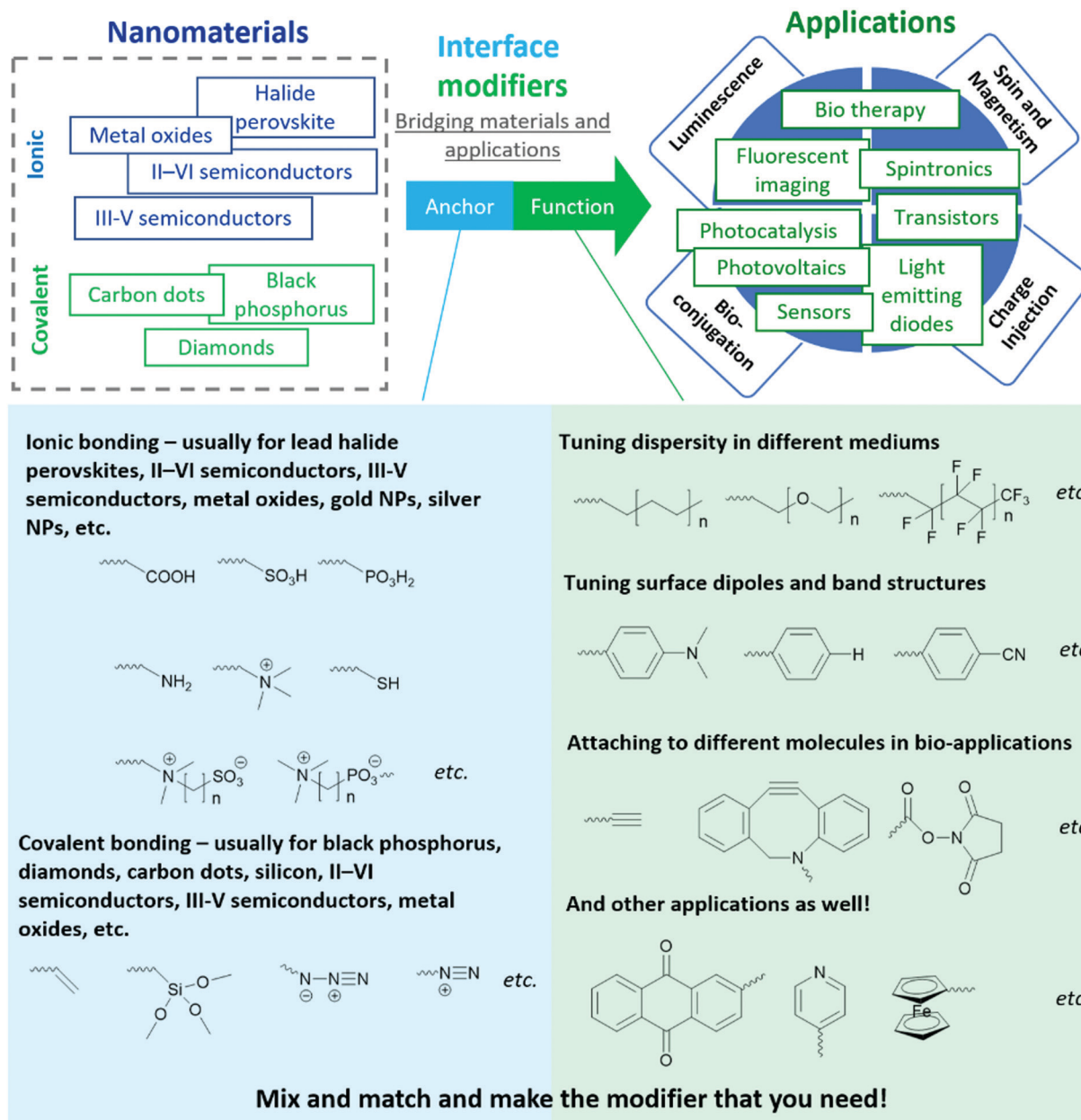
Fig. 1 An interface modifier can be seen as molecule comprised of two key components: (i) anchor groups that attaches to inorganic nanomaterials, and (ii) functional groups that tune the properties of inorganic nanomaterials to better suit the target applications. Some examples of anchors and functional groups are shown here.

two-electron donor, the X-type one-electron donor (species that are one-electron neutral ligands, but two electron donors as anionic ligands), and the Z-type two-electron acceptor Lewis acid (Fig. 2).[39] The above criteria are the fundamental perspectives on "anchor" component for II–VI QDs, III–V QDs, metals, metal oxides, IV–VI QDs, and I–III–VI NCs materials. In the following section, representative examples will be presented and illustrate the primary mechanisms of ligand exchange for each material and surface type to better elucidate the "anchor-functionality" paradigm.

L-type ligands coordinate to electron-poor sites on the NC surfaces. The most common L-type NC capping ligands are

amines, phosphines, phosphine oxides, thiols, and carboxylic acids (Fig. 2). These ligands are neutral and passivate stoichiometric facets or charge neutral sites of a NC surface. For ligand exchange performed in nonpolar solvents, there is no charge barrier to L-type ligand dissociation. As a result, L-type ligand exchange generally occurs through a dissociative pathway to relieve steric crowding, yielding a dynamic surface of bound and unbound ligands.[38] Two materials that can employ L-type species as native ligands during synthesis are CdSe (II–VI) and $CuInS_2$ (I–III–VI). Both provide interesting examples of L-L-type ligand exchange. In an early example, Meijerink and co-workers used the quenching of CdSe photoluminescence to study L-type

Fig. 2 Classification of ligand anchor groups on representative metal chalcogenide (ME) NCs.

ligand exchange from native amine, phosphine, and phosphine oxide ligands to thiols.[40] The exchange of native amines with thiols was shown to be the most facile, while the exchange with phosphines and phosphine oxides occurred more slowly. Amines, phosphine oxides, and thiols compete to bind to the cadmium surface sites, while the phosphines bound to surface selenides must dissociate to allow the thiol to coordinate to a nearby cadmium. Additionally, the bulkier phosphine and phosphine oxide anchor groups are proposed to slow ligand exchange and prevent nearby surface-ligand interactions.[40] More recent studies on CdSe surface chemistry and ligand exchange add additional nuance to these conclusions. For example, it is now understood from NMR spectroscopic investigations that phosphines bind the Lewis acidic metal sites on QD surfaces, rather than perturbing the chalcogenide oxidation states.[41] Quantitative ^{1}H and ^{31}P NMR experiments also report contradicting steric and electronic effects on ligand affinity to QD surfaces. The more electron-rich phosphines show a higher affinity for CdSe QD surfaces than isostructural amines, but bulkier ligands have a lower binding affinity despite having more electron-donating substituents due to repulsive interactions between the ligands. Hens and co-workers reported charge-neutral CuInS$_2$ NCs synthesized with octadecylamine and studied ligand exchange with *in situ* variable temperature NMR experiments.[42] Unlike the dynamic surfaces of common L-bound NCs, the amines remained tightly bound at room temperature but became dynamic at higher temperatures. Maintaining charge neutrality at the surface, the amine ligands were shown to exchange with L-type thiols but not with X-type carboxylates during a multi-step ligand exchange in a nonpolar solvent at elevated temperatures. A study of another I–III–VI material, CuInSe$_2$, reported the exchange of L-type amine and phosphine native ligands with thiols or other phosphines assisted by the addition of a charge-neutral Z-type I$_2$ ligand, which is necessary to displace the tightly bound native ligands.[43] Z-type ligands were found to exchange with L-type amines in II–VI and IV–VI NCs as well.[44–46]

Ligand binding is also influenced by facet-dependent surface composition, which is presented here with studies of materials with native X-type ligands. NMR and FTIR techniques have been used to identify chelating and bridging carboxylate X-type ligands passivating the polar {100} and {111} facets of CdSe NCs, while the nonpolar {110} facet is weakly coordinated by modified Z-type cadmium carboxylates.[47] PbS NCs showed a similar pattern, where the Pb-rich {111} facets were passivated with X-type oleate and hydroxide ligands, while the stoichiometric {100} facets, which do not require any charge balance, were coordinated by L-type oleic acid.[38] Atomically precise semiconductor clusters also provide defined platforms for elucidating ligand binding.[45,48] L- and X-type binding modes of carboxylates on InP surfaces were quantified with an analytical ^{1}H NMR method using InP magic sized clusters, and partial X-X-type ligand exchange was shown with thiolates and phosphonates. Phosphonates are known to strongly bind and replace carboxylates in CdSe QDs as well.[49] Carboxylic acids passivate metal oxides such as HfO$_2$ and ZrO$_2$ in nonpolar solvents by separating into a carboxylate and a proton, which bind as two separate X-type ligands (sometimes referred to as X$_2$-type) under basic conditions.[50] The basicity of surface oxygen ions in metal oxides allows protons to act as ligands, and the resulting dissociative carboxylic acid binding allows for the exchange of the neutral X$_2$-type with L-type ligands.[51]

The binding affinity of specific anchor groups to different NC surfaces can also be predicted by the hard/soft acid base principle. Within II-VI and metal oxide NCs, surfaces with harder Lewis acidic cations such as Zn^{2+} in ZnSe or ZnO tend to bind to harder bases such as OH$^-$,[52] the softer Cd^{2+} cations of CdTe bind to softer ligands such as HS$^-$, and CdSe and CdS NCs of intermediate polarizability are ligated by both hard and soft bases.[53] The covalency of the lattice affects the classification of the metal sites because the hard acid In^{3+} behaves as a softer acid in InP and InAs NCs due to the increased sharing of charge density. The strong soft-acid/soft-base bond formed by Au and S means that thiolates are common native ligands for Au NCs. These ligands can be easily exchanged for other soft ligands, but Au NCs are not stabilized by harder anchor groups.[53,54] Au, Ag, and other metal NCs are commonly synthesized with capping ligands for stability and in the scope of the ligands discussed above for stabilization in nonpolar solvents. Generally, thiols and phosphines give higher stability for metal NCs than amines, carboxylic acids, and alcohols.[55]

An exciting recent addition to the nanomaterial surface characterization toolbox is isothermal titration calorimetry (ITC), which can elucidate ligand binding and exchange thermodynamics by quantifying the heat changes upon addition of a ligand titrant.[56] ITC can detect ligand binding over a wide range of particle concentrations in their native solvent environment, allowing the results to be compared to both optical and NMR spectroscopy data. As discussed above, NCs often have multiple facets with potentially different binding enthalpies that could be resolved in ITC data. ITC measurements and associated time-trace analyses allowed Greytak and co-workers to identify a two-step ligand exchange

and association mechanism for the exchange of native carboxylates with alkylphosphonates on CdSe QDs and to extract thermodynamic parameters.[56] The first set of ITC signals included a fast exothermic curve followed by fast endothermic line shape. The authors assigned the exothermic process to the X-type ligand exchange of carboxylates for phosphonates, while the endothermic signal was tentatively attributed to a rapid proton exchange between the incoming and outgoing ligands. Then, after a stoichiometric amount of phosphonate for X-type exchange, the ITC signals changed to a slower exothermic response that was assigned to the L-type association of phosphonic acid to a second set of surface sites. Additional studies of ligand exchange by ITC report the effects of ligand chain length and NC size on the exchange thermodynamics.[57–59] ITC measurements of the exchange of native oleate with alkylthiols of various chain lengths on CdSe QDs report an enthalpy–entropy compensation effect that maintains near-constant Gibbs free energy.[57] The longer chain ligands have stronger inter-ligand van der Waals interactions that lead to increased exothermicity. This increase is mitigated by a loss of entropy from restricted chain conformations and in this case, an elimination of the disorder caused by the double bond in oleate. The study also investigated the effects of particle size on ligand-exchange thermodynamics and reported a less favourable exchange for larger NCs, an observation that was explained by the ability to more closely pack ligands on the larger, less curved NC surfaces. Alivisatos and co-workers reported an endothermic exchange of native straight chain carboxylates with oleic acid, also attributed to stronger inter-ligand interactions and higher ordering of longer, fully saturated ligand chains.[58] Moving beyond semiconductor QDs, ITC measurements of the binding of thiols to gold NC surfaces showed an increase in binding enthalpy with increasing chain length accompanied by a larger loss of entropy, following the previously mentioned enthalpy–entropy compensation effect.[59] The Au-thiol system also showed more favourable ligand binding with smaller-sized NCs, understood by the increased ratio of edge sites to facet surface sites.

2.1.2 Lead halide perovskites. In 1958, metal-halide perovskites were found to have unusually high and tuneable photoconductivity.[60] This observation inspired investigation of these materials as absorbing and charge-separating materials for dye-sensitized solar cells,[61–67] which in turn inspired a broad and ongoing effort to use these materials in next-generation solar technologies. Compared to the materials shown in Section 2.1.1, perovskite lattices possess higher ionicity, and therefore, require a matching ionicity in the "anchor" component in the "anchor-functionality" design – utilizing highly polar cationic and anionic structures in most cases. Such understanding was critical for the fabrication of single-layer perovskite solar cells with power conversion efficiencies (PCEs) of 25.6%,[68] perovskite-perovskite tandem cells with a 24.8% PCE,[69] and perovskite-silicon tandem cells with a 29.15% PCE.[70] Such promising results inspired an expansion of perovskite research to colloidal nanocrystalline versions of the same materials,[36,71–75] and these have now been used in applications such as LEDs,[3,76,77]

lasers,[78–81] X-ray detectors,[82,83] luminescent solar concentrators,[84–88] and single-photon sources.[89–91] These applications are enabled by the high defect tolerance of perovskite NCs[92–95] and their broad spectral tunability with anion[96–98] and cation[99–103] alloying. Many researchers have found that the high ionicity of metal-halide perovskites often leads to degradation of their favourable photoluminescence,[104–107] hindering their use in several important research areas. Fortunately, it has been shown that these NCs can be effectively stabilized and passivated by carefully considering their surface structure and designing anchor groups that accommodate their lattice.

The first reported synthesis of colloidally stable perovskite NCs used a combination of oleylamine and oleic acid, as shown in Fig. 3a.[36] Methylammonium is a key component of thin-film perovskites, and early reports demonstrated that longer chain alkylammonium molecules have high potential as defect passivating groups for perovskite solar cells.[108,109] These results suggest that ammonium ions are a critical anchor group for stabilizing the surfaces of perovskite NCs, a hypothesis that was confirmed by NMR studies that show that oleylammonium oleate groups are the main anchor groups that coordinate with perovskite NC surfaces, rather than oleylamine and oleic acid.[1] This study and other explorations of ligand-NC binding[110,111] show that perovskite NC-ligand interactions are far weaker than those of II–VI and III–V semiconductor NCs,[38,42,112] despite these materials having very high photoluminescence quantum yields (PLQYs). These high PLQYs were explained by DFT studies that demonstrate that most perovskite defect structures produce trap states that do not lie within the material's bandgap,[94,95] but it was later shown experimentally[71] and with DFT[113] that undercoordinated lead sites at terminal surfaces or grain boundaries are critical defects that may be responsible for reduced NC PLQY. These studies inspired a large amount of synthetic and ligand chemistry investigations to improve perovskite NC PLQY and increase overall NC stability *via* passivating such lead sites.

Early on, it was noted that bromide ions play a critical role in ligand desorption reactions by coordinating with ammonium ions in solution.[1] This idea – along with the attribution of low NC PLQY to undercoordinated lead[71] – led researchers to explore routes to add additional halide anions to passivate these defects, considering that halides are native lead-coordinating components in perovskite lattices. From the NC synthesis perspective, the original $PbBr_2$, Cs oleate injection synthesis has been supplemented with methods that involve an injection of alternative halide sources, such as benzol halides,[98,114] trioctylphosphine-halides,[115] and trimethylsilyl halides[96,116,117] into solutions of Cs and Pb oleates. Additionally, excess halide can be added in the form of $ZnBr_2$.[118] This allows more precise control of ion ratios to improve NC PLQYs from synthesis. Post-synthetic treatment with excess lead bromide,[119] and halide containing ligands such as didodecyl dimethylammonium bromide (DDABr)[14,120,121] and oleylammonium halide[122] also improve the PLQY and stability of perovskite NCs. This treatment with DDABr and other similar ligands has proven effective, and the quaternary ammonium
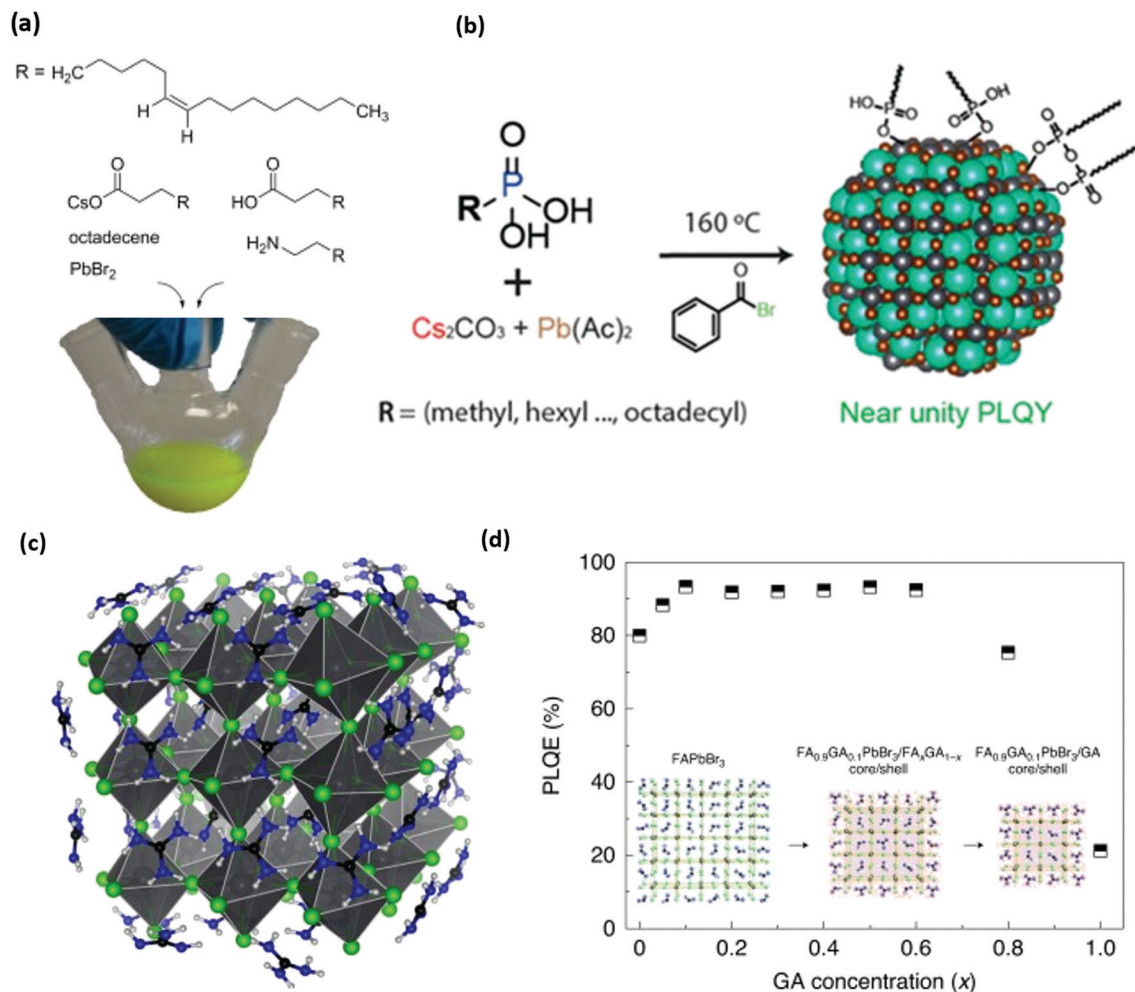
Fig. 3 (a) Structure of organic and inorganic precursors typically used to synthesize perovskite NCs. (b) Structure and scheme for the synthesis of perovskite NCs without any cationic ligands. Phosphonic acids are used to dissolve precursors and stabilize NC surfaces. (c and d) Molecular structure of guanidinium (GA) stabilized perovskite NCs and photoluminescence quantum efficiency (PLQY) of synthesized NCs as a function of GA content. Panel a reproduced with permission from ref. 1 and 2, panel b reproduced with permission from ref. 130, and panel c reproduced with permission from ref. 2 and 3.

bromide has become a popular perovskite NC passivating group.[96,106,116,123–125]

Other researchers have focused on alternative anchor groups for perovskite materials. Phosphonate and phosphine groups have exposed lone pair electrons that have shown high potential as passivating groups for thin-film perovskites.[126,127] Trioctylphosphine was occasionally used to help dissolve lead precursors for hot injection syntheses,[36] but was further explored to show that trioctylphosphine[128] and trioctylphosphine oxide[129] can be used to improve NC stability and PLQY. It was even shown that NCs with traditional ligands could be recovered by simply treating the NCs with trioctylphosphine.[130,131] This recovery is presumably due to an L-type association of electron pairs on phosphine or phosphine oxide moieties with the under-coordinated Pb^{2+} sites that are typically associated with low NC PLQY.[93,132] The hypothesis was verified for perovskite thin films by studying the effect of film treatment with electron pair containing thiophene and pyridine,[133] and a thorough study of DFT and experimental results from anionic ligand exchanges showed that softer Lewis base anions such as phosphonates, fluorinated carboxylates, and sulfonates are effective passivating groups for the soft Lewis acid character of undercoordinated lead.[93] Such results explain the high performance of phosphonate and sulfonate containing zwitterionic ligands.[115,134] More recently, it has been shown that phosphonic acid groups can be used as the sole ligand for synthesizing $CsPbBr_3$ as described in Fig. 3b. The resulting phosphonic capped $CsPbBr_3$ achieved near-unity PLQY confirming excellent passivation of surface traps.[135,136] These studies reinforce the idea that soft Lewis bases are effective anchor groups for passivating critical halide vacancies on perovskite NC surfaces.

The cationic ligand anchor group has not received as much research attention as the anionic or charge-neutral anchor groups. Most studies of perovskite materials only investigate variations on primary amines[1,36] and quaternary ammonium ions.[14,120,121,137] DFT studies suggest that N–H moieties exhibit hydrogen bonding character between the ammonium cation and the halide anions in bulk methylammonium[138,139] or

formamidinium[140] lead halide perovskite materials. Hydrogen bonding has been explored as an important NC stabilization factor for ammonium ligands[141] and formamidinium cations,[142] but some recent reports now investigate the favourable effect of guanidinium[143] and pyrazine[144] on the perovskite's properties. Recently, guanidinium was shown to be an important surface ion in the synthesis of perovskite NCs for the highest efficiency green-emitting perovskite LED reported so far, an advance that was enabled by the increased PLQY with guanidinium shown in Fig. 3c.[3] These promising results motivate the further investigation of ligand hydrogen bonding character and guanidinium passivation as strategies to understand and enhance the performance of metal-halide perovskites in future applications.

2.2 Anchor groups for covalent lattices

As demonstrated in Section 2.1, the "anchor-functionality" paradigm emphasizes the use of anchors matching the chemical environment of nanomaterials surface to achieve efficient binding and effective surface passivation. In Section 2.2, we discuss covalent lattices, and therefore also the different organic building blocks that can form covalent bonds to these covalent lattice surfaces. Like Section 2.1, there are differences in ionicity in these covalent lattices as well, and they require different bond forming strategies. For example, on silica surfaces, the strong electronegativity of oxygen atoms compared to silicon atoms leads to the formation of polar Si–O bonds, which is significantly different from covalent bonds by atoms of similar electron negativities, such as Si–Si bonds and Si–C bonds. Therefore, in this section, we categorize the examples according to such variance to better illustrate and emphasize the "anchor" section criteria in the "anchor-functionality" paradigm – matching the chemical environment of the nanomaterial surface.

2.2.1 Si–O bonds on interfaces. Silica encapsulated NCs have become increasingly important for biomedical, catalytic, and optoelectronic applications due to their enhanced stability and biocompatibility, suppression of fluorescence quenching by surface adsorbates or redox-active molecules, and ability to be post-synthetically functionalized for a wide variety of end-uses. Other advantages of silica shells include their ability to be easily processed and tailored by controlling their size and porosity over a wide range.[145–148]

The growth of silica shells on NCs has been extensively studied, with two predominant methods emerging: the Stöber method and the reverse microemulsion method, as shown in Fig. 4. In the first method, silica shells are formed directly on the surface of the NC seeds by replacing the stabilizing ligands with silica precursors. In an early example, Mulvaney and coworkers introduced bifunctional (3-aminopropyl) trimethoxysilane to citrate-stabilized gold particles in aqueous solution.[149] The –NH$_2$ coordinates to the gold surface and the –Si(OEt)$_3$ groups extend outward, allowing the formation of a silica layer on the gold NCs. This method can also be used to achieve ultra-thick silica shells *via* seeded-growth using small silica-coated particles as seeds and tetraethyl orthosilicate

(TEOS) as a typical precursor of silicon alkoxides.[150,151] Water-in-oil (W/O) microemulsion or reverse microemulsion is another technique to encase NCs in silica. In this method, NCs are introduced to stable W/O microemulsions or nanodroplets of organic solvent, water, and surfactants. Upon successive additions of TEOS and ammonia, hydrolyzed TEOS replaces the surfactants on the NC surface and the silanization process is initialized. Compared with the classical Stöber method, the reverse microemulsion method allows more control over silica nucleation, final particle size, and monodispersity since the particles are contained in small, stable, and narrowly distributed nanometer-sized droplets in a continuous phase.[152] More detailed discussion on the synthesis of silica-coated NCs, metal oxide NCs, and metal NCs can be found in recent review articles.[153–155]

Besides acting as a shield to protect NCs from surface oxidation and ripening, silica shells can also serve as a platform for surface modification and functionalization (Fig. 4). The outer surfaces of silica-coated NCs are rich in silanol, which can act as a handle to covalently attach various functionalized organosilanes to modify the surface with different functional groups. For example, Qin and co-workers prepared superparamagnetic Fe$_3$O$_4$ NCs encapsulated in an amine-functionalized silica shell using (3-aminopropyl) triethoxysilane.[156] By using amino groups as reactive handles, polymerization of glycidyl methacrylate was initiated at the surface, and the resulting particles were successfully utilized for lipase immobilization. For thiol-functionalized silica coated NPs, the density of thiol groups on silica shells can be tuned by varying the ratio of methyltriethoxysilane, *n*-propyltriethoxysilane, and 3-mercapto-propyltriethoxysilane. By coating magnetite NCs with different thiol-functionalized silica shells, Kessler and co-workers demonstrated heavy metal uptake processes for wastewater treatment.[157] Carbonyl groups were also attached by modifying amine groups on silica surfaces with succinic anhydride.[158] The carbonyl-functionalized silica-encapsulated gold particles subsequently form covalent bonds with oligonucleotides when EDC is present (see mechanism with EDC details in Section 3.3.1) to detect gastric cancer. Furthermore, chloroalkyl alkoxysilanes are widely used to terminate the silica surfaces with chlorine atoms, which serve as leaving groups for the introduction of other functional groups. Utilizing this method, Veisi and co-workers replaced the chlorine atoms on silica surfaces with isoniazide moieties, which immobilize Pd catalysts on the silica surface. The resulting Fe$_3$O$_4$@SiO$_2$/isoniazide/Pd catalysts successfully facilitated Suzuki coupling reactions at room temperature.[159]

In addition, click chemistry handles can also be attached to silica surfaces (a more detailed discussion of click chemistry is included in Section 3.3.4). Typically, silica-coated Fe$_3$O$_4$ particles are bromine-functionalized with (3-bromopropyl)trichlorosilane and further treated with NaN$_3$ to achieve azide-functionalized nanoparticles.[160,161] Some applications of these azide-functionalized magnetic nanoparticles have been demonstrated for click immobilization of mono-alkyne metalloporphyrin to obtain free-base porphyrin conjugate,[161] and gold NC modified porous paper working electrode, and magnetic silicon NC with
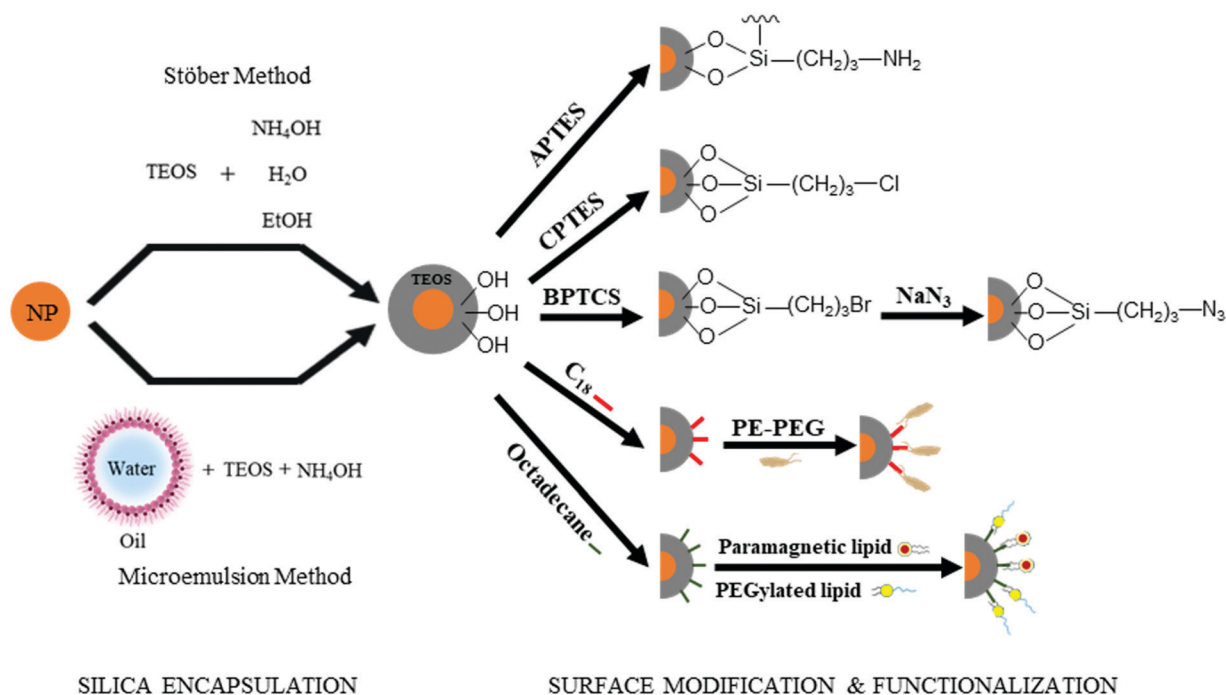
Fig. 4 Silica encapsulation of nanoparticles (orange) can be achieved by two main methods: the Stöber method and the microemulsion method. The surface of the silica shell is rich in hydroxyl groups, which can be modified and functionalized by silane coupling agents, polymers, or lipids. APTES = (3-Aminopropyl)triethoxysilane; CPTES = (3-Chloropropyl)triethoxysilane; BPTCS = (3-Bromopropyl)trichlorosilane.

protein.[160] Thiol groups are another common click chemistry handle applied as an intermediate to functionalize the surface of silica shells. In the work of Shahsavarifar and coworkers,[162] click reactions between thiols and acrylic acid groups were used to form a functional group for immobilizing molybdenum complexes on silica-coated magnetite nanoparticles to prepare a recoverable molybdenum catalyst. The resulting catalyst showed a high catalytic activity and selectivity in the epoxidation of olefins and allylic alcohol. Click chemistry handle-functionalized silica shells can also be achieved by modifying the Stöber method; By using a mixture of TEOS and a click-handle-functionalized triethoxysilane, for example (3-azidopropyl)triethoxysilane or O-(propargyloxy)-N-(triethoxysilylpropyl)urethane in the Stöber method, azido- or alkyne-functionalized silica-coated nanoparticles can be prepared in a one-step procedure.[160–162]

The silanol surface can also be directly coated by small biological additives or polymers without silane coupling reagents. Riedel et al. coated Au@SiO$_2$ with bovine serum albumin, a blood albumin protein derived from cows, for chemotherapeutic applications.[163] The stability and biocompatibility of NCs in harsh chemical treatments including strong acids can also be guaranteed by dual encapsulating with silica and polymers. Hu et al. combined silica and amphiphilic polymer coating techniques to prepare ultra-stable NCs, which can be used for biosensing in a broad range of chemical conditions.[164] Mulder and co-workers made bio-applicable and target-specific NCs coated with silica and a dense monolayer of lipids without the use of silane coupling agents.[165,166] These particles were suitable for both fluorescence imaging and

MRI studies, and showed highly specific uptake by human umbilical vein endothelial cells.

2.2.2 Modification of H- and O-terminated silicon and diamond surfaces. Silicon and diamond share intrinsically robust mechanical properties, high thermal conductivity, low biotoxicity, chemical inertness, and can be doped to obtain p-type or n-type semiconductors. In their NC forms, the surfaces of these materials can be further tailored for their desired application. Native surface functionalization is determined during material production, as processing conditions lead to surface passivation with hydrogen or oxygen moieties such as hydroxyl and carboxyl groups.[167,168] Silicon nanoparticles (SiNPs) passivated with hydrogen are obtained from synthesis and purification methods that require hydrogen-rich atmospheres (e.g., NH$_3$, H$_2$) or hydrogen-containing precursors (e.g., SiH$_4$) and etchants (e.g., HF, NH$_4$F).[169–171] While most methods result in H-termination, oxide layers form when SiNPs are exposed to oxygen-rich environments.[172,173] Unlike SiNPs, the production of nanodiamonds (NDs) often results in an amorphous carbon layer or a strained sp^2-hybridized carbon shell of graphene (buckydiamond) or graphite (carbon 'onion').[174–176] These shells arise from the direct synthesis of NDs[177] or form during the ball-milling of bulk diamond, regardless of initial passivation.[174–176,178,179] Acid- or gas-etching techniques purify the NDs and remove the carbon shell, resulting in hydrogen or oxygen termination with anhydrides and carboxyl groups.[180,181] The deliberate hydrogenation or oxidation of oxygen-terminated surfaces requires thermal annealing, UV, or plasma treatments in the presence of the respective targeted atomic, molecular, or

plasmonic atmosphere. In addition to dry methods, wet chemical methods and electrochemical reduction/oxidation can be employed to exchange H-terminated surfaces with oxygen, and *vice versa*. It is worth mentioning that one can terminate the surfaces of silicon and diamond with other atoms through similar methods, resulting in F, Cl, Br, N, and S termination. However, they are not as commonly used as H or O terminated surfaces and thus not included in this tutorial review. The fabrication of these surfaces and their modification methods have been comprehensively reviewed.[32,182]

These hydrogenated and oxygenated surfaces are excellent templates for further surface modification, as they can be subjected to a variety of different environments and chemistries to achieve adsorption and covalent anchoring of molecules. This section will provide a mechanistic overview of subsequent techniques employed to further modify these surfaces. These modified surfaces allow for material compatibility within drug delivery,[183–186] sensing,[184,187] catalysts,[188,189] electrochemistry,[188,189] and tribology,[190,191] amongst other applications.

Instances of the direct adsorption of molecules onto hydrogenated SiNP or ND surfaces are limited. H-terminated silicon and diamond have weak surface dipoles,[192,193] making the surfaces averse to hydrogen bonding, dipole interactions, or physisorption. Unlike H-terminated SiNPs and ND, O-terminated surfaces have more pronounced surface dipole moments that facilitate hydrogen bonding and dipole–dipole interactions.[194] This is observed through the nanomaterial's stability in aqueous environments; hydrogen bonds form between the partially positively charged hydrogen atom of water ($H^{\delta+}$) and terminal oxygen atoms with a partial negative charge ($O^{\delta-}$). While hydrogen bonding and dipole interactions are prevalent, electrostatic interactions *via* ion exchange reactions with carboxyl functionalized surfaces have also been observed. In neutral environments, carboxyl groups deprotonate to form charged carboxylate anions, which associate with cations in solution, such as protonated amino groups of proteins[168] and with cationic polymers.[195]

However, these electrostatic bindings between organic molecules and inorganic surfaces break down easily due to their weak binding strengths. Therefore, the anchoring of molecules to the surfaces of SiNPs and NDs is more preferably and more commonly achieved through covalent bond formation *via* the functional groups on the surface (*e.g.*, hydrogen or oxygen moieties such as hydroxyl, ether, carbonyl, and carboxyl groups). Organic molecules are grafted onto the surface of silicon and diamond through a variety of methods such as alkene/alkyne addition,[196,197] silanization,[191,198] diazonium chemistry,[32,199,200] esterification,[201] and other reactions. Similar to exchanging hydrogen with oxygen and *vice versa*, these methods rely on a combination of the following strategies: (1) withdrawing surface atoms to generate dangling bonds, (2) withdrawing ionized electrons from the surface, or (3) chemical reactions with surface moieties. These strategies have been grouped accordingly in Fig. 5.

The chemical functionalization of the H-terminated surfaces of silicon and diamond can be achieved through thermal, photochemical, or electrochemical grafting of α-olefins.[196] Three methods have been reported: radical chain reaction (RCR), photochemical grafting, and electrochemical grafting.

Initiation of RCR requires cleavage between H atoms and C or Si atoms on the surface to form reactive surface dangling bonds (free radicals) that react with the terminal double bond of the incoming organic molecules, covalently grafting the organic molecules to the particle's surface.[202] The H–Si or H–C bond cleavage is achieved with a radical initiator (*e.g.*, diacyl peroxide) that abstracts hydrogen from the material's surface. The resulting radical attaches the double bond of the α-olefin and forms an intermediate secondary alkyl radical. Propagation occurs as the secondary alkyl radical abstracts an adjacent hydrogen atom from the silicon or diamond surface, therefore producing a new surface dangling bond and continuing the chain reaction.

Alternatively, the photochemical grafting of α-olefin requires irradiation with UV light instead of a radical initiator.[196] It was first applied to functionalize H-terminated silicon, and later translated to H-terminated diamonds.[32] The photochemical mechanism of this method starts with an electron transfer from Si or diamonds to incoming α-olefins under UV excitation, forming a positively charge Si or C center at the surface and an alkyl anion. The nucleophilic alkyl anion attacks the positively charged center at the surface and forms a covalent bond.[203,204] Similar to photochemical grafting, anodic and cathodic electrochemical grafting through electron transfer and grafting of terminal alkanes and alkynes has been utilized for doped semiconducting SiNPs and ND.[197] Such photochemical and electrochemical grafting of α-olefin has been applied to other H-terminated nanomaterials (*e.g.*, Ge and B particles),[205,206] metal surfaces,[207] and other carbon allotropes.[202] Covalent grafting of terminal alkenes introduces various terminal functional groups (*e.g.*, –NHCOCF$_3$, –NHCOO(*tert*-butyl), –COOCH$_3$, –CH$_3$, –COOH) onto the material's surface to provide new functional properties, or to serve as reactive handles for further modification.[205,206,208–210]

Diazonium chemistry can be used to functionalize either hydrogenated or oxygenated surfaces with covalently bonded aromatic organic compounds.[32,196] The material's surface donates electrons to reduce the electron-withdrawing diazonium salt (Ar–N$_2^+$), forming an aryl radical (Ar•) and molecular nitrogen (N$_2$). Electron-rich donating surfaces are achieved through the injection of electrons (cathodic electrografting) or through electron ionization. The former method requires the material to be conductive and is only applicable to doped SiNPs or NDs. Due to the surface dipole of the H-terminated diamonds, the resulting band bending raises the conduction band of H-terminated diamond above vacuum level. Therefore, when an electron is either injected or excited onto the conduction band, such a high-lying conduction band provides sufficient offset for efficient electron transfer from diamonds to diazonium salts.[26] Regardless of the method, the produced aryl radical attacks and displaces the native surface group, forming a surface radical. Radical recombination occurs, covalently grafting the aryl radical to the surface of the SiNP or ND. Similar to other methods, diazonium salts introduce a wide

Fig. 5 (a) Examples of different functional groups introduced to silicon or diamond surfaces through different surface modification techniques; (b) surface modification of silicon or diamond surface *via* radical pathway; (c) surface modifications of silicon or diamonds *via* electrochemical pathways.

range of terminal functional groups (*e.g.*, –COOH, –Br, –NO$_2$, –CN, –NH$_2$) to the surfaces of these nanomaterials, enabling further chemistries or molecular anchoring.[211] Furthermore, covalent attachment *via* diazonium reactions has also been displayed for other inorganic NCs (*e.g.*, TiO$_2$, Fe$_2$O$_3$, Fe, Au, Cu, Ni)[199,200,212–215] and carbon allotropes.[216]

Chemical reactions with moieties on the O-terminated surfaces are also effective in creating covalent bonds with incoming organic molecules. Hydroxyl groups on surfaces can be modified through silanization chemistry, passivating the material's surface with siloxide. Considering that the surface of O-terminated SiNPs is silica, please refer to Section 2.2.1 for further description of this functionalization method. Alternatively, SiNPs and ND surfaces with carboxyl groups can be subjected to amidation or esterification reactions. Carbodiimide reagents (commonly EDC or DCC) activate the carbonyls to form an intermediate complex that is susceptible to nucleophilic attack by primary amines or hydroxyl groups. This process is also commonly utilized to graft proteins and biomolecules directly to the surfaces

of SiNPs or NDs, which will be discussed in the following bio-medical section (Section 3.3), but can also be used to covalently bind NPs to polymers for electrochemical applications.[201,217,218] It is worth mentioning that this esterification is also feasible in modifying the surfaces of graphene quantum dots, considering the large number of carboxyl groups on their surfaces.[219]

3. Functional groups for enhanced performance

In Section 2, the different chemical interactions that anchor groups utilize to attach to a variety of nanomaterials was discussed. In this section, we will elaborate on the roles of the functional group element of the "anchor-functionality" paradigm, with an emphasis on the interactions between functional groups and the original nanomaterials or their surroundings, through which they further enhance the performance of the original nanomaterials.

3.1 Tuning dispersity for different applications

Due to their small sizes, most inorganic nanomaterials can be dispersed into solution and form a meta-stable colloidal dispersion. This enables processing with low-cost and efficient solution-based techniques, such as inkjet printing or roll-to-roll printing, to manufacture different electronic devices (e.g., solar cells,[11] LEDs,[220] photodetectors[221]) at room temperature, in contrast to the high-temperature and/or high-vacuum techniques used to process traditional inorganic materials. Usually, to accelerate drying of the printed devices, volatile organic solvents are used and the ligands of such nanomaterials are often comprised of long alkyl chains as functional groups to increase their solubility in organic solvents.[222] On the other hand, by choosing hydrophilic functional groups, resulting inorganic nanomaterials can be dispersed into aqueous solution and be injected into living organisms as nanomedicines.[34] Regarding dispersity, the functional groups in the "anchor-functionality" design offer camouflage for nanomaterials to fit into different environments.

The dispersity of a ligand-modified nanomaterial is governed by the interaction between the solvent molecules and the ligand shell, following the similarity–intermiscibility theory, which is more well-known by the "like dissolves like" principle.[223,224] Solvent molecules prefer to interact with molecular domains sharing a similar polarity, and thus the solute dissolves better in solvents that are structurally similar.

The interactions between solutes and solvents can be classified into three categories, – non-polar, polar, and protic/ionic, as exemplified in Fig. 6 by the different ligands used in lead halide perovskite NCs to tune their solubility in different solvent mediums. These ligands possess the same zwitterionic anchor groups. Therefore, it is implied that the difference in dispersity originates from the different functional groups. To facilitate the dispersion in non-polar solvent, Kovalenko and co-workers pair a long alkyl chain ($-C_{18}H_{37}$) with a zwitterionic anchor group for perovskite NCs.[115] The long alkyl chain only consists of non-polar hydrocarbon moieties, which is similar to the chemical structure of non-polar solvents such as benzene, toluene and hexane. Therefore, the resulting capped perovskite possesses good solubility in non-polar solvents due to the favorable intermolecular interaction between the alkyl chain and the solvents. When polar groups are introduced into a ligand, for example, the ester groups in ZP3,[225] the resulting perovskite NCs can be dispersed in polar solvents such as ethyl acetate and butyl acetate, which are known to be anti-solvents for alkyl-capped perovskite. When the ligand is modified by functional groups that are able to form hydrogen bonds, for example, the polyethylene glycol (PEG) and carboxylate groups in ZW-PIMA-PEG, it enables NC

Fig. 6 The structure of different ligands for perovskite QDs and the solvents used to disperse the QD–ligand composites. Anchor groups are labeled red, non-polar groups are labeled black, polar groups are labeled green, and H-bonding reactive groups are labeled blue. Due to the increasing interaction intensity in the order of non-polar interaction, to polar interaction and to H-bonding interaction, the stronger interaction dominates when two or more types of interactions are present.

dispersion in ethanol.[226] Moreover, there have been examples of aqueous dispersion of perovskite NCs, where much longer PEG chains of more than 100 repeating units were applied to facilitate the solvation of NCs in water.[226–228] There are many other examples of functional groups and solvents in each category that are not listed here, and it is always important to be able to identify the interaction mechanism of the functional groups and solvents when designing a ligand for inorganic nanomaterials.

3.2 Optoelectronic applications

Optoelectronics is one of the most studied properties of inorganic nanomaterials. In Section 3.2, we discuss using organic building blocks to tune or enhance the performance of inorganic nano-materials, by elucidating the steric and electronic interactions between ligands and nanomaterials. Through these examples, we present the basic selection criteria for functional groups in the "anchor-functionality" design.

3.2.1 Shifting energy levels. Because of the high surface area to volume ratio of NCs, anchor and functional groups can be used to tune the electronic structure of the NC material. Anchor groups are typically quite important for passivating surface defects to improve PLQY, but surface binding molecules can also change the band energies of the corresponding NC. The presence of insulating NC ligands is known to limit the performance of NC-based devices,[229,230] but it was also hypothe-sized that band level modification could be helpful to improve device performance.[231] This effect was investigated in meso-porous TiO$_2$-based devices, where the high surface areas of the inorganic material allow for tuning of the materials' band structure with surface treatments of organic molecules. It was initially shown that the band energies of the TiO$_2$ anode of a solar cell could be tuned by adding carboxylate functionalized polymers.[232] The effect was explained by the creation of a surface dipole that shifts the work function of the TiO$_2$, an effect that impacts the open circuit voltage of the final device. This was further verified by exploring a variety of benzoic acids with different functional groups to systematically tune the surface dipole and band energies of TiO$_2$.[229,230,233]

Ligands with dipole-inducing functional groups have now been heavily explored as interfacial modifiers for a variety of inorganic materials. Dipole-induced vacuum level shifting was used to explain improved thin-film perovskite solar cell performance,[109] but functional-group-based energy level tuning was critical to the development of PbS photovoltaics. The interfacial dipole's potential as an important electronic tuning tool was best exemplified by a screening of 12 different ligating molecules, which showed that the band energies of PbS could be tuned by a full electron volt by changing the dipole of the surface functional group.[30] Further explorations based on solution-state ligand exchanges expanded this range to 2 eV, and explained this change using the dipole of the ligand and the effects of ligand interdigitation on band energies (Fig. 7).[31] This motivated research to tune the band energies of PbS and CdSe for organic–inorganic solar cells with functional group engineering.[234,235] Additionally, Sargent and co-workers made
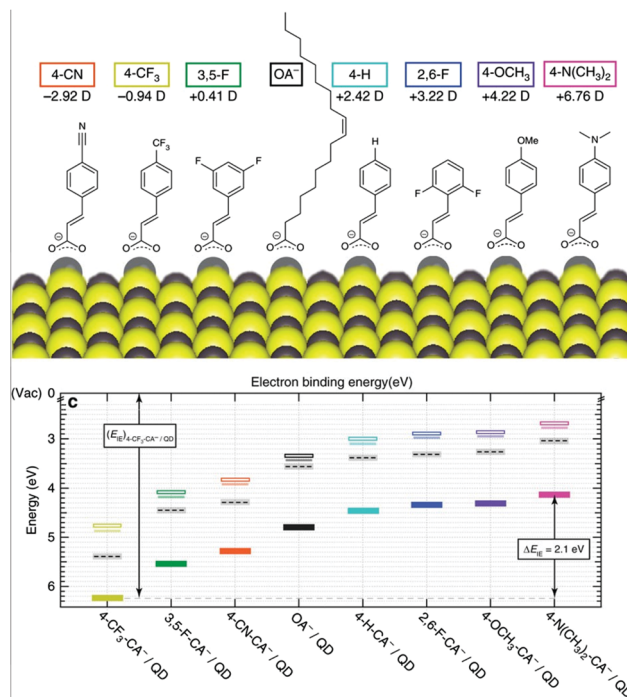

Fig. 7 (Top) The molecular structures of organic molecules on PbS QDs and their dipole intensity; (bottom) the shifting of energy levels from the surface treatments with the dipole molecules determined by UPS. Reproduced with permission from ref. 31.

the impressive innovation of creating a bulk PbS hetero-junction solar cell by combining PbS NCs functionalized with different ligands in the same device.[236] By respectively using thioglycerol and methylammonium iodide[237] as ligands for PbS, the band offsets between these two resulting NCs were engineered to create a bulk heterojunction solar cell with a PCE of 10.7%. This method of device fabrication was further optimized to yield devices with PCEs of 13.3%.[238] Such innovations demonstrate the exciting and unique opportunities for functional-group-induced band engineering of inorganic NCs.

3.2.2 Energy and charge transfer. When studying a NP/ligand system, charge and energy transfer between the two can be modulated by tuning the NP itself, the charge/energy accepting moiety on the ligand, and the link between these. With such a wide array of strategies to modify these dynamics, ligand tuning can provide detailed mechanistic information about these fundamental processes.

3.2.2.1 Charge transfer. When ligands act as charge acceptors or donors, they should have frontier orbitals energetically aligned to accept or donate electrons to the NP. If fast and efficient charge transfer (CT) is desired, frontier orbitals of the ligand or band edges of the NP (see Section 3.2.1) should be tuned such that there is a driving force for charge transfer ($-\Delta G_o$ in Fig. 8a). Analysis of the rate of charge transfer, k_{ct}, may be framed in the context of Marcus theory.[239] A 2013 review by Knowles and co-workers aggregated several studies that vary the driving force for charge transfer.[240] Within each data set, k_{ct} increases with increased driving force, corresponding to the
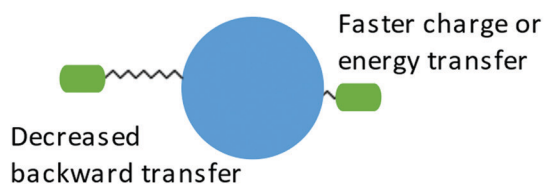
(a) Energy alignment
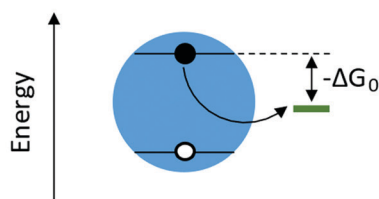
(b) Spectral overlap
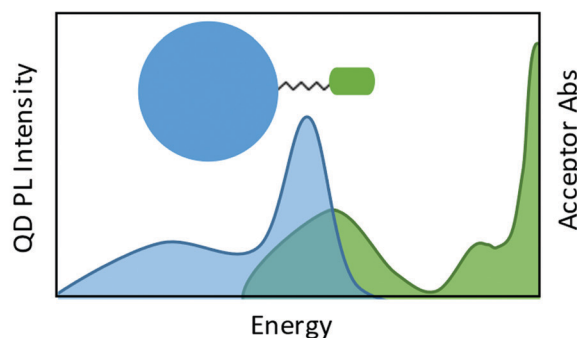
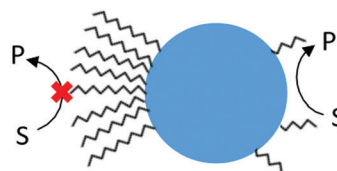## (c) Physical separation

(d) Substrate permeability

Fig. 8 (a) Scheme showing that proper energetic alignment allows a driving force for electron transfer. (b) Overlap between the quantum dot photoluminescence spectrum and the energy accepting ligand absorbance spectrum is required for energy transfer. (c) Physical separation between the nanocrystal core and the energy or charge accepting moiety can control the rate of forward, and by extension, backward transfer. (d) Long, dense ligand shells can prevent substrate access to the nanocrystal. Shorter, less dense ligands allow close interaction between the nanocrystal and substrate, promoting catalysis.

Marcus normal region.[240] At present, the Marcus inverted region has not been observed in NP-ligand CT systems.

Both organometallic[241,242] and conjugated organic moieties[243–245] may have their energy levels tuned through substituents to achieve desired energy alignment with the NP. Organometallic complexes that contain an anchor group to bind to the NP may act as charge localizing ligands because of multiple low energy redox states. These include ferrocene derivatives[246–249] that act as model charge localizing centers and catalytically competent complexes (see Section 3.2.3). Organometallic ligands are especially interesting because the metal center may have multiple oxidation states, allowing for multiple charges to transfer per ligand.[250] Conjugated organic molecules containing an anchor group are also good candidates for charge localization including viologens,[251] quinones,[252] and fused-ring arenes.[253] In such ligands, the conjugated organic moiety acts as a charge acceptor to create long-lived, highly delocalized radicals.

There are additional characteristics that influence charge transfer besides the driving force. An increased distance between the NP and the charge localizing center decreases the rate of charge transfer, as highlighted in Fig. 8c.[254–257] The anchor group may also be important to charge transfer. In 2017, Olshansky and co-workers reported on a CT system that was described by surface trap-mediated transfer rather than Marcus two-state direct transfer, highlighting the importance of the NP/ligand interface.[248] The head group of the ligand may relax quantum confinement or create charge carrier traps, both

of which influence charge transfer to the rest of the ligand or to external substrate.[258] By extension, the charge localizing center of the ligand may itself be viewed as an additional charge carrier trap.

3.2.2.2 Energy transfer. The study of energy transfer from NCs began with investigations of Förster resonance energy transfer (FRET) systems. Because of the strong distance- and orientation-dependence of FRET efficiency, FRET can be used as a "spectroscopic ruler".[259] This ability to estimate of distances and orientations of molecules has made FRET a common tool for studying conformational changes in biomolecules.[260] In a QD-ligand system, the donor chromophore is photoexcited and transfers energy to an acceptor chromophore (photoresponsive adsorbates such as dye-labeled peptides) through a non-radiative process.[261] Important considerations for FRET systems are the spectral overlap of the donor emission and acceptor absorption and the physical separation between the NC and the photoresponsive ligand (Fig. 8b and c). A 2008 perspective from Medintz and Mattoussi outlines the basis for use of NC FRET systems for sensing and biological applications.[262]

An emerging use of NC energy-transfer systems is photon up-conversion *via* triplet–triplet annihilation. The NC acts as the photosensitizer, readily forming a spin–forbidden triplet state due to strong spin–orbit coupling. This triplet is transferred in a Dexter-type energy transfer to a triplet transmitter ligand, and then transferred again to an unbound annihilator.[263] The 2017

perspective by Huang and Tang proposes that the bottleneck to efficient triplet–triplet annihilation is the efficiency of the triplet energy transfer from the NC to the transmitter ligand.[264] Optimization of this step requires energy alignment of the triplet states to the photosensitizer and annihilator, a short distance from the NC to the transmitter core, and strong binding between the NC and transmitter. The triplet transmitter ligand is typically composed of a head-group to bind to the NP and a highly conjugated organic group to act as a stepping-stone between the NC and the annihilator.

3.2.3 Photocatalysis. QDs,[265–267] perovskites,[268–270] metal oxides,[271,272] and metal NCs[273,274] have been widely explored as sensitizers and catalysts for photoredox reactions in recent years. There have been numerous strategies employed to improve catalytic performance, such as utilizing engineered defects[275] and heterostructured architectures.[276] One approach that stands out as simple yet effective is tuning the ligand shell.

The ligand shell is a physical barrier that can be easily manipulated to enhance access of substrates to the NP surface. From a ligand coverage perspective, it has been shown that a less dense ligand shell enhances catalysis, likely explained by increased "permeability" facilitating interaction between substrates and NP surfaces (Fig. 8d). For example, a study by Chen *et al.* showed that zwitterionic ligand-capped $CsPbBr_3$ QDs with a surface coverage of 3.0 nm^{-2} (compared to 5.4 nm^{-2} for oleate- and oleylamine-capped NPs) exhibited an increased rate of stereoselective C–C oxidative homocoupling of α-aryl ketonitriles.[277] From a similar permeability argument, the Weiss group has shown that a mixed ligand shells enhance C–C coupling between 1-phenylpyrrolidine (PhPyr) and phenyl *trans*-styryl sulfone.[278] Furthermore, there are numerous reports demonstrating that shorter ligands are better for catalysis.[279] Shorter ligands decrease the steric bulk at the NP surface, and if charge transfer proceeds *via* an electron-tunnelling mechanism, shorter ligands can increase the rate of this transfer.[280] In fact, some studies show that a NP passivated with small inorganic ligands,[281] or a NP with a completely bare surface,[282] is actually better for catalysis. This therefore begs the question, does the presence of ligands ultimately hinder catalysis? Surface ligands have been at the forefront of the long-standing conflict between maintaining colloidal stability and impeding charge transfer, but we argue that they are most certainly necessary and can be designed intentionally to be advantageous in catalysis.

As mentioned in Section 3.2.2, NP surface ligands can be non-innocent in the context of charge separation. Upon photo-excitation, one of the main competing pathways between charge transfer to a substrate is recombination. This pathway can be avoided by prolonging this excited state and promoting charge transfer by engineering a trap state at a ligand site. This can serve the dual purpose of spatially separating the electron and the hole to prevent recombination in the NP and bringing the charge carrier closer in proximity to substrate. This has been shown particularly in the context of hole-quenching ligands,[283] which is significant since hole transfer is widely believed to be rate-limiting in photocatalysis.[284] For instance,

3-mercaptopropionic acid (MPA) and other thiol capping ligands are often used as ligands on NP photocatalysts because they are able to quench photogenerated holes due to their mid-gap highest occupied molecular orbital (HOMO) levels.[285] In another study, a known hole acceptor, phenothiazine, was ligated onto the surface of CdSe QDs to dramatically improve H_2 evolution rates.[286] Similar effects have also been observed with conductive ligands that facilitate electron transfer to substrate. Beard *et al.* showed that $CsPbBr_3$ NCs functionalized with short, cinnamate ligands display enhanced electron-donating ability to benzoquinone by up to ∼23x, and an increased activity for α-alkylation of aldehydes.[287] Given these findings, we can imagine an idealized Janus particle system wherein one facet is bound by hole-quenchers and the other by electron-acceptors, to achieve precise and controlled separation of charge carriers for a photoredox event.

Ligands can play an even more active role in photocatalysis by directing reaction pathways through interactions with substrates and intermediates, which can ultimately impact product selectivity. In a system where the NP acts as a photosensitizer, metal complex catalysts can be anchored onto the surface. This has been demonstrated by a ruthenium oxygen-evolution reaction catalyst bound to CdS nanorods.[288] In two examples of electrostatic immobilization, a $[Ni(terpy)_2]^{2+}/CsPbBr_3$ composite was synthesized, where the Ni(II) complex acted as an electron sink for CO_2 reduction.[289] Similarly, a cationic ruthenium species was self-assembled onto the surface of negatively charged Au NPs to catalyze the transfer hydrogenation of acetophenone.[290] Substrates themselves have also been shown to transiently bind to the surface of CdSe QDs and form diastereoselective products.[291] In the [2+2] cycloaddition of 4-vinylbenzoic acid derivatives, selectivity for the minor *syn*-cyclobutane products was achieved by a proposed mechanism of triplet–triplet energy transfer following binding to the surface at the carboxylate functional group.

Finally, ligands can greatly increase the stability of the photocatalyst. Hole-quenching amines have been shown to displace native ligands *in situ* and confer greater activity and stability to CdS QDs.[292] When anisotropic materials are used, ligands can also help maintain the unique morphology of the NPs.[293] This is particularly important because speciation of the NP post-catalysis often reveals aggregation and degradation.[284] Being able to maintain the catalyst during operation has great implications for benchmarking, fully understanding what the active photocatalyst is, and painting an accurate overall picture of reaction rate and mechanism.[294,295]

3.2.4 Chiral-ligand interaction. Colloidal NC functional groups can also be tuned to modify the spin properties of the underlying material.[296] The mechanism by which chirality occurs in NCs has been associated with: (i) orbital hybridization or close range dipolar Coulomb interactions between the energetic levels in the chiral ligands and the achiral NCs (ii) near-surface chiral distortion (or defects) of the NC due to ligand interaction and (iii) ligand aggregation in a chiral pattern on the NC surface.[297–302] For example, this effect was observed in the functionalization of CdSe and CdS with

L-cysteine, where the chiral nature of the functional group induces energy level splitting, through a hybridization between the hole energy level of the NC and the ligand's HOMO (mechanism i), which can be probed through circular dichroism.[303] This suggests that chiral ligands can be used to tune NC energy splitting to spin-selective optical and transport properties. Such potential was demonstrated by the use of chiral ligands to produce NCs with enantiomerically selective catalytic activity,[304] an innovation that has been leveraged to fabricate biosensors based-on chiral ligand-functionalized NCs.[305] In another instance, Cu_2S NCs are transferred chirality through adsorbed D-/L-penicillamine ligands arranging on the surface in a chiral pattern (mechanism iii), which allows for selective protein and peptide cleavage for improved protein engineering.[306]

Furthermore, given the promising spin coherence properties of perovskite materials,[21,307] researchers have begun exploring the possibilities for tuning perovskite spin properties with chiral ligands. For instance, two-photon absorption upconverted chiral photoluminescence in $CsPbBr_3$ NCs with enantiomeric ligands was observed, where the chirality was attributed to mechanism ii.[302] He and co-workers engineered chirality in perovskite NCs by varying the amount of ligand. They found that with high concentration of the functional group, geometric aggregation of the ligands induces chiroptical properties (mechanism iii), while at lower concentrations, surface distortion/defects contribute to chirality (mechanism ii).[301] This chiral effect was realized for perovskite devices when α-phenylethylamine groups were used in the synthesis of 2D perovskites to produce spin-selective photodetectors that can differentiate left and right circularly polarized light.[302] Similarly, these chiral-functionalized 2D perovskites have been used to fabricate a circularly polarized white LED.[308] This device concept was further optimized and chiral 2D perovskites have now been used as spin selective hole injection layers for perovskite NC-based circularly polarized LEDs with a room-temperature electroluminescent efficiency of 2.6%.[309] These impressive devices based on chiral ligand functionalization are important for the future of spintronic applications of inorganic nanomaterials, but more research regarding the impact of ligand structure on performance should be conducted to advance this field.

3.3 Bio-medical applications

Different from optoelectronic applications, where functional groups directly enable new functionality in inorganic nanomaterials, in bio-medical applications, functional groups in the "anchor-functionality" design act as linkers that bind nanomaterials to different biomolecules, and it is the incoming biomolecules that enable new properties of the resulting bioconjugates. For example, proteins or peptides on the surface of QDs can be used to control their self-assembly,[310,311] or enable selective interaction between QDs and specific small molecules[312] or macromolecules,[313] which are essential for chemical sensors, target drug delivery and different bioimaging techniques. These new properties of the resulting bioconjugates originate from the inherent structural or special recognition

properties of the biomolecules.[310,311] Bioconjugation methods are dependent on the functional groups on both the nanomaterial surfaces and the incoming biomolecules, as briefly summarized in Fig. 9. However, biomolecules, such as proteins and peptides, contain complicated structures and a large number of functional groups compatible with different bioconjugation methods. To avoid ambiguity in discussion, in this review, we took a different perspective and categorized the research cases by chemical interactions instead of by applications, to better illustrate the intrinsic and fundamental aspect of bioconjugation reactions – chemical bond formation.

3.3.1 Targeting biomolecules containing carboxyl groups. The carboxyl group is the most common handle used to form bioconjugates, considering its wide availability, for example, on the C-terminus of proteins and peptides, O-terminated diamonds, graphene oxides, carbon dots, and some commercial quantum dots.[314] Plus they can be easily obtained by treating inorganic surfaces with ligands that contain carboxyl groups.[33]

Among the methods for carboxyl bioconjugation, electrostatic interaction is the simplest approach. Carboxyl groups are negatively charged in aqueous environments, which matches well with typical positively charged proteins. For example, trypsin is a positively charged enzyme in the small intestine that digest proteins. Gole *et al.* used a carboxylate-rich polymer to coat the surface of gold nanorods, which endowed the gold nanorods with negative charges.[315] The bioconjugation between the modified gold nanorods and trypsin was carried out by simple mixing in solution. However, it was observed that the bioactivity of the trypsin was reduced to 19%. Gole *et al.* ascribed this reduced performance to alteration of the protein secondary structures when it is associated with a charged surface,[316] and protein immobilization.[317] On the other hand, Gole *et al.* also applied a zero-space linker (EDC as shown in Fig. 9) to covalently link the carboxylate-rich gold nanorods to trypsin, *via* the amine groups on the trypsin surface as handle. However, this bioconjugation method with EDC leads to even lower bioactivity of trypsin, which is 13%. This can be ascribed to the acidic nature of EDC, and it requires an excessive amount to achieve a high conversion rate. The resulting low pH environment may lead to irreversible change in the secondary structure of trypsin.

The above results emphasize the importance of maintaining the pH environment in bioconjugation reactions. To better preserve the bioactivity of trypsin, Gole *et al.* also experimented with "click" chemistry methods to form bioconjugation without altering the pH environment. As a result, the bioactivity of trypsin was better preserved to 53%. A small decrease of the bioactivity after binding to gold nanorod may be inevitable due to immobilization of the protein. It is worth mentioning that "click" reactions are popular in biochemistry research due to their high bio-orthogonality, which is crucial to maintain the bioactivity of biomolecules. A detailed discussion of "click" reactions will be later discussed in Section 3.3.4.

3.3.2 Targeting biomolecules containing amine groups. Amine is another functional group often applied as handles to crosslink biomolecules to inorganic surfaces. They are
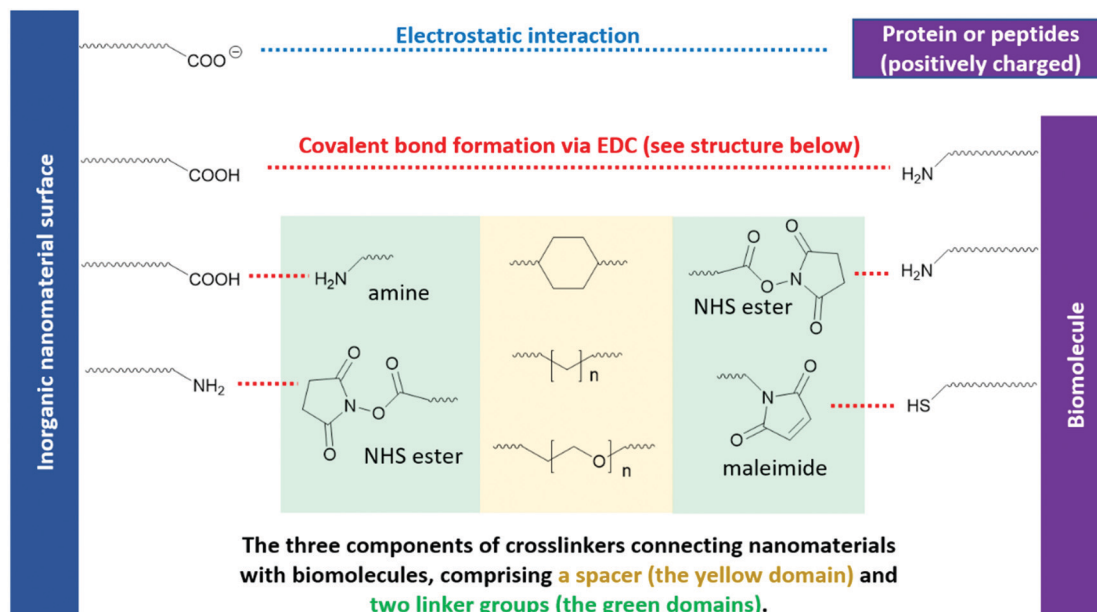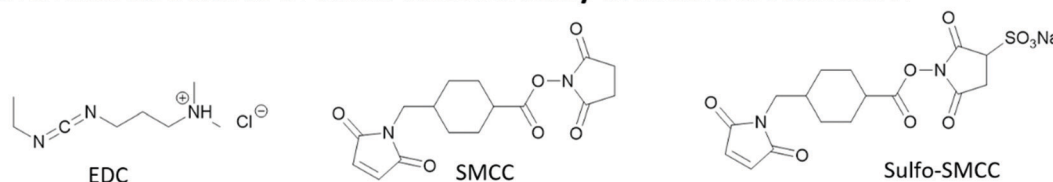
Fig. 9 Reaction handles on inorganic nanomaterials and biomolecules commonly used in bioconjugation reactions and the structures of some commercial linkers for bioconjugation.

available at the N-termination of proteins and peptides, the sidechain lysine, and inorganic nanomaterials functionalized with an amine-terminated silica surface (see Section 2.2.1). Though there are many functional groups able to react with amine that can potentially serve as a crosslinker, many of them have limited selectivity and readily form covalent bonds with non-target functional groups. For example, the epoxide group can form a covalent bond with amine groups in mild-pH aqua environments *via* a nucleophilic pathway, which suggests that it would be a good choice for bioconjugate synthesis. However, the epoxide group is also highly reactive towards other nucleophiles in biomolecules, such as thiol and hydroxy. This leads to undesired intramolecular crosslinking within a biomolecule and/or aggregation among several nanomaterial bioconjugates, both of which are detrimental to their bioactivity. In addition, most anchor groups to ionic surfaces, discussed in Section 2.1, are nucleophiles and reactive towards the epoxide group as well. To our knowledge, the epoxide group has only been applied to silica-coated nanomaterials to form bioconjugates,[318] benefited from the inert nature of silica shell.

N-Hydroxysuccinimide (NHS) esters have low toxicity[319] and are generally considered to be primary-amine-specific,[320] making it a good crosslinker for amine groups. The reaction between NHS ester and a primary amine is nucleophilic, where the primary amine is the nucleophile attacking the NHS-activated ester bond.

Although thiol and hydroxide groups are nucleophiles as well, it is demonstrated that NHS ester only reacts with the thiol and hydroxide groups in biomolecules when NHS ester is present in excess.[320,321] Therefore, one can achieve a high selectivity of amine-NHS-ester reaction by controlling the amount of NHS ester added. Fig. 9 shows a commercial bio-crosslinker functionalized with NHS ester, SMCC, which also has a maleimide handle (see Section 3.3.3) to link to other nanomaterials or biomolecules.

Due to the hydrophobic nature of the NHS ester, crosslinking reactions are usually conducted in organic solvents, which may perturb the bioactivities of biomolecules. To enable crosslinking reactions in physiologic solutions, sulfonated versions of NHS ester crosslinkers are designed and commercially available, for example sulfo-SMCC shown in Fig. 9. Furthermore, the formation of amide bond between NHS ester and the primary amines in biomolecules can be carried out at pH 7–8, demonstrating high biocompatibility. In lower pH environments, protonation of primary amines take place, which reduces their nucleophilicity and thus their reactivity towards NHS esters. In higher pH environments, the stability of NHS ester decreases, due to the relatively higher concentration of the nucleophilic hydroxide group. The half-life of NHS ester drops from 4–5 hours at pH 7, to 1 hour at pH 8, and to 10 mins at pH 8.6.[322,323] However, the half-life of the resulting amide bonds is very stable

in water, in the range of 7 years,[324] rendering it a reliable method in constructing bio-conjugates.[322,323]

3.3.3 Targeting with biomolecules containing thiol groups. Compared to the previously discussed carboxyl and amine groups, fewer thiol groups are available in typical biomolecules. Thiols are available in cysteine-containing proteins and peptides. In addition, thiols can be readily applied as a functional group to the surface of inorganic nanomaterials as discussed in Section 2.2.1. Due to its high nucleophilicity, thiols are very effective handles in bio-conjugation reactions.

Maleimide is the most popular crosslinker for thiols, due to their exceptionally fast kinetics and high selectivity towards the thiols on cysteine. A variety of maleimide-based crosslinkers available commercially, for example, SMCC and sulfo-SMCC in Fig. 9. The fast kinetics of maleimide towards thiols can be ascribed to its lower lowest unoccupied molecule orbital (LUMO) levels, due to the electron-withdrawing imide group and the strained five-member ring – which facilitates its orbital interaction with the non-bonding orbitals of thiols and therefore bond formation.[325]

The nucleophilic reaction between thiol and maleimide readily occurs at near-neutral conditions, pH 6.5–7.5.[314] At pH above 8, the hydrolysis of the imide group takes place, which leads to the ring-opening of maleimide. This ring-opening reaction is problematic in bioconjugations. First, it

destroys the strained five-member ring of maleimide and yield undesired products that are non-reactive toward thiols. Second, the hydrolysis of the newly formed maleimide-thiol adduct eventually leads to the breakdown of the bioconjugation. Although amine is also a nucleophile, its reaction with maleimide is negligible due to its much slower kinetics, only 1/1000 of thiol.[314] This explains the high selectivity of maleimide towards cysteine in proteins and peptides. There are other bioconjugation methods for thiol as well. However, they are not as widely applicable as maleimide due to low selectivity and/or slow kinetics and are therefore not included in this tutorial review. For those who are interested, please refer to the reviews by Koniev *et al.*[325] and Ochtrop *et al.*[326]

3.3.4 Targeting with non-natural bio-active molecules using click chemistry. In the previous three sections, we discuss the three functional groups in natural proteins and peptides that can serve as handles for bioconjugation reactions. However, nucleic acids, the primary information-carrying molecules in cells, lack such reactive handles.[33] To address this, non-natural nucleotides bearing bioconjugation handles are introduced onto the nucleic acid backbones.[327] Some of the commercially available non-natural nucleotides are shown in Fig. 10.[328]

Click chemistry handles (*e.g.*, azide, alkyne, and alkene) are popular in non-natural nucleotides for the following two

1) Examples of commercially available non-natural nucleotides with click chemistry handles

EdU   EdC   EU   AU   EdA   EdG

2) Examples of commercially available non-natural amino acids with click chemistry handles

azide-alanine   azide-phenylalanine   alkyne-alanine

3) Examples of commercially available bioconjugation linkers with click chemistry handles

azide-NHS-ester linker   strained-alkyne-NHS-ester linker   alkyne-NHS-ester linker

Fig. 10 Examples of commercially available non-natural nucleotides, non-natural amino acids and bioconjugation linkers functionalized with click chemistry handles. The click chemistry handles are highlighted red, the structural analogs of natural nucleotides and amino acids are highlighted green, and the handles attaching to amino groups (as discussed in Section 3.3.2) are highlighted blue.

reasons. First, click chemistry reactions possess the advantages of fast kinetics, high yield, bio-orthogonality, and applicability in aqueous solvents. Second, click chemistry handles do not exist in natural biomolecules and possess high selectivity towards their coupling partners, which is critical to eliminate the side reactions during the synthesis of nucleic acids, and further increase the selectivity of subsequent bioconjugation reactions. For similar reasons, click chemistry is also widely applied in protein and peptide bioconjugation, starting with the non-natural amino acids shown in Fig. 10. It is worth mentioning that in addition to biomolecules, click chemistry handles can also be applied to inorganic nanomaterial surfaces (see Section 2) and crosslinkers as shown in Fig. 10. Two types of click chemistry reactions attract most attention in bioconjugation methods: azide–alkyne cycloaddition and inverse electron-demand Diels–Alder cycloaddition.

3.3.4.1 Click chemistry: azide–alkyne cycloaddition. Copper(I)-catalysed azide–alkyne cycloaddition (CuAAC) has fast kinetic rates in the range of 10–100 M^{-1} s^{-1},[329] high selectivity and almost quantitative yields,[330,331] which are advantageous for bioconjugation. However, due to the biotoxicity of Cu(I) compounds and their insolubility in aqua solution, concerns were raised regarding the biocompatibility of CuAAC. The small amount of Cu(I) required in bioconjugation reactions, which is in the μM range, has demonstrated to impair the functionality of biomolecules by promoting the generation of reactive oxygen species.[332,333] Efforts have been focused on reducing the toxicity of Cu(I) complex and increasing their aqueous solubility. With an appropriate ligand design, Bevilacqua *et al.* demonstrated CuAAC can be performed in living cells.[334]

Strain promoted azide–alkyne cycloaddition (SPAAC) is a way to bypass the biotoxicity of Cu(I) compounds, as SPAAC does not require catalysts due to the higher activity of the strained alkyne group. However, these reactions have much slower kinetics, in the range of 10^{-3}–1 M^{-1} s^{-1},[329] depending on the level of strain applied to alkyne group, which is linear when free standing.[335] Fig. 11 shows the different SPAAC alkyne. Due to the flexible nature of sp^3 carbons in the eight-member ring, the alkyne group in OCT is under a low level of strain, which leads to a low reaction rate of 2.4×10^{-3} M^{-1} s^{-1}. With 4 rigid sp^2 carbons atoms in the eight-member ring, the reaction rate of DIBAC is increased to 0.31 M^{-1} s^{-1}. BARAC possesses one more sp^2 carbon compared to DIBAC, by changing the methylene group in DIBAC into carbonyl group, and therefore its reaction rate is further increased to 0.96 M^{-1} s^{-1}.[335] However, it is worth pointing out that the increased strain at the alkyne group also increases its activity towards thiols, reducing the bio-orthogonality of this method.[335,336]

3.3.4.2 Click chemistry: inverse electron-demand Diels–Alder cycloaddition (IEDDAC). IEDDA reaction stands out from other bio-orthogonal reactions considering its unmatchable kinetics (as much as 10^6 M^{-1} s^{-1})[329] and its excellent orthogonality and biocompatibility. IEDDAC is a subcategory of Diels–Alder
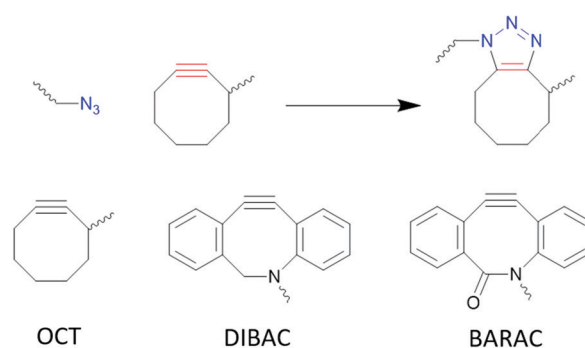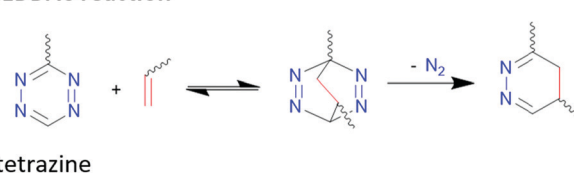

Fig. 11 Reaction schemes of different click chemistry reactions.

reaction, characterized by a [4+2]-cycloaddition between a diene (usually tetrazine derivatives) and a dienophile (alkynes or alkenes), and subsequent evolution of 1 equivalent of nitrogen that pushes the equilibrium to one end and eliminates the reversible nature of Diel–Alder reactions, as shown in Fig. 11.

Although strain on alkynes and alkenes can promote the reaction rate of IEDDAC, it is not necessarily required. Oliveria *et al.* demonstrated a successful bioconjugation between terminal-alkene-functionalized protein and tetrazine, with a kinetic rate of 0.21 M^{-1} s^{-1},[337] which is comparable to SPAAC reactions. Nevertheless, faster reaction kinetic are preferred in bioconjugations, and strained alkynes and alkenes are often paired with tetrazine for such purposes. Transcyclooctene (TCO) moiety is one of the most common strained alkenes used, and its reaction with tetrazine reaches a rate of more than 1000 M^{-1} s^{-1} in organic solvents.[338] In addition to strain, electronic effects, steric effects, solvent, and pH have significant impacts on the kinetic of IEDDAC, which have been discussed comprehensively by Oliveria *et al.*[329]

4. Conclusion and outlook

In this tutorial review, we coalesce a wide range of examples and concepts regarding inorganic nanomaterial surface functionalization into the streamlined "anchor-functionality" paradigm. To help the reader better understand this idea, the functions of different anchor groups and functional groups were elaborated with examples covering a variety of material types and

applications. In Section 2, the different interactions between inorganic surfaces and organic anchors were discussed, and it was demonstrated that the selection of anchor groups is determined by the chemical features of the inorganic surfaces, such as lattice type and bonding motif. In Section 3, the roles of functional groups were discussed focusing their mechanisms on enhancing and/or endowing new functionalities of inorganic nanomaterials to optimize their performances in certain applications.

Although the types of materials and applications covered in this review are somewhat specific, the chemistry methods discussed are not limited to the examples mentioned. For example, Section 2 discussed using diazonium chemistry to graft organic molecules to only silicon and diamond. In fact, diazonium chemistry has also been used to modify other inorganic materials with covalent lattices, such as black phosphorus,[339] WS_2, $MoSe_2$, WSe_2,[340] and Ni_2P.[341] The covalent characteristics these materials share allow the use of the same chemistry for surface modification. On a broader scope, the silanization chemistry used to modify O-terminated silicon and diamond surfaces applies to cellulose as well, because all of these material surfaces are functionalized with hydroxyl groups.[342] This highlights the importance of identifying the chemical features of a surface prior to modification, and meanwhile provides a useful mindset for modifying other novel materials emerging in the future. Similarly, the functionalities that organic building blocks can introduce are not limited to the categories in Section 3. For example, the ethylene oxide moiety has been successfully introduced to ligands, forming crosslinking ligand shells and providing good oxygen and water insolation for lead halide perovskite NCs.[343] (2,2,6,6-tetramethylpiperidin-1-yl)oxidanyl, commonly known as TEMPO, is magnetic resonance (MR) active due to its radical nature. When introduced to surfaces of fluorescent QDs, the resulting TEMPO-QD complex makes a bimodal MR/optical imaging reagent providing high signal-to-noise ratios.[344] Considering the structural flexibility of organic compounds, the choices of functionality are extensive and leave much room for exploration.

Interdisciplinary collaborations can not only consummate certain existing ideas as stated above, but also establish the foundation for a new research domain. Take the recent surge of chiral spintronics research as an example.[309,345,346] Chiral spintronics utilize the connection between the electron spins (a quantum physics concept) and the chirality of organic compounds (a chemistry concept), which is their mirror-reflection asymmetry as shown in Fig. 12. Moving spins can couple to a chiral object *via* spin–orbit coupling. When the spin possesses the same handedness as the chiral object, it can travel a longer distance. Such hybridization with chiral structures not only removes the requirement of an external magnetic field in traditional spintronics, but also leads to significantly larger spin currents compared to other spin–orbit-coupling-based devices from the achiral counterparts. Such enhancement is crucial to achieve higher signal-to-noise ratios and reduce electricity consumption. Currently one of the topics of interest in

Fig. 12 The mirror-reflection asymmetry comparison between electron spins and chirality of chemical compounds. The small blue arrows and the big blue arrows respectively represent the moving directions and spinning directions of electrons. The red arrows indicated the chirality of two lactic acid enantiomers. The direction of the red arrow is defined by the arrangement of the functional groups around the chiral centers (marked with "*"), with the order of −OH > −COOH > −CH₃.

chiral spintronics is introducing chiral ligand to QD surfaces, leveraging the quantum confinement effect to obtain robust spin states at room temperature and chiral effect to enhance spin current.[309] This case exemplifies the fact that the organic–inorganic interface is a hybrid domain that requires the fusion of knowledge from multiple scientific disciplines *via* familiarizing a broad range of introductory content regarding organic building blocks to researchers from non-organic-chemistry backgrounds. We hope that by sharing this anchor-functionality paradigm with interdisciplinary researchers, we can spark other novel collaborative ideas in these communities.

Author contributions

Y. H. and C. K. L. led and coordinated the writing of this paper. Y. H. wrote Sections 1, 3.1, 3.3, and 4. T.A.C. wrote Sections 2.1.2, 3.2.1, and 3.2.4. B. M. S. wrote Section 2.2.2. Y. H., T. A. C., and B. M. S. combined, formatted, and proofread the manuscript. H. L. wrote Section 2.1.1. H. A. N. wrote Section 2.2.1. M. K. H. wrote Section 3.2.2. F. Y. D. wrote Section 3.2.3. L.M.J. and T. A. C. wrote Section 3.2.4. B. M. C., D. R. G., and C. K. L. supervised the writing. All authors provided critical feedback and helped shape the manuscript.

Conflicts of interest

There are no conflicts to declare.

Acknowledgements

Notes and references

1 J. De Roo, M. Ibáñez, P. Geiregat, G. Nedelcu, W. Walravens, J. Maes, J. C. Martins, I. Van Driessche, M. V. Kovalenko and Z. Hens, *ACS Nano*, 2016, **10**, 2071.

2 C. B. Murray, D. J. Norris and M. G. Bawendi, *J. Am. Chem. Soc.*, 1993, **115**, 8706.

3 Y.-H. Kim, S. Kim, A. Kakekhani, J. Park, J. Park, Y.-H. Lee, H. Xu, S. Nagane, R. B. Wexler, D.-H. Kim, S. H. Jo, L. Martínez-Sarti, P. Tan, A. Sadhanala, G.-S. Park, Y.-W. Kim, B. Hu, H. J. Bolink, S. Yoo, R. H. Friend, A. M. Rappe and T.-W. Lee, *Nat. Photonics*, 2021, **15**, 148.

4 A. Ekimov and A. Onushchehko, *ZhETF Pis ma Redaktsiiu*, 1981, **34**, 363.

5 R. Rossetti, S. Nakahara and L. E. Brus, *J. Chem. Phys.*, 1983, **79**, 1086.

6 J. Zhou, Y. Yang and C.-Y. Zhang, *Chem. Rev.*, 2015, **115**, 11669.

7 C. Tan, X. Cao, X.-J. Wu, Q. He, J. Yang, X. Zhang, J. Chen, W. Zhao, S. Han, G.-H. Nam, M. Sindoro and H. Zhang, *Chem. Rev.*, 2017, **117**, 6225.

8 X. Wang, Z. Bao, Y.-C. Chang and R.-S. Liu, *ACS Energy Lett.*, 2020, **5**, 3374.

9 E. Jang, S. Jun, H. Jang, J. Lim, B. Kim and Y. Kim, *Adv. Mater.*, 2010, **22**, 3076.

10 J. Y. Kim, J.-W. Lee, H. S. Jung, H. Shin and N.-G. Park, *Chem. Rev.*, 2020, **120**, 7867.

11 G. H. Carey, A. L. Abdelhady, Z. Ning, S. M. Thon, O. M. Bakr and E. H. Sargent, *Chem. Rev.*, 2015, **115**, 12732.

12 H. Guan, S. Zhao, H. Wang, D. Yan, M. Wang and Z. Zang, *Nano Energy*, 2020, **67**, 104279.

13 Z. Wang, Y. Liu, S. Zhen, X. Li, W. Zhang, X. Sun, B. Xu, X. Wang, Z. Gao and X. Meng, *Adv. Sci.*, 2020, **7**, 1902688.

14 J. Pan, L. N. Quan, Y. Zhao, W. Peng, B. Murali, S. P. Sarmah, M. Yuan, L. Sinatra, N. M. Alyami, J. Liu, E. Yassitepe, Z. Yang, O. Voznyy, R. Comin, M. N. Hedhili, O. F. Mohammed, Z. H. Lu, D. H. Kim, E. H. Sargent and O. M. Bakr, *Adv. Mater.*, 2016, **28**, 8718.

15 H. Moon, C. Lee, W. Lee, J. Kim and H. Chae, *Adv. Mater.*, 2019, **31**, 1804294.

16 K. Wu and T. Lian, *Chem. Soc. Rev.*, 2016, **45**, 3781.

17 G. Liu, C. Zhen, Y. Kang, L. Wang and H.-M. Cheng, *Chem. Soc. Rev.*, 2018, **47**, 6410.

18 V. Biju, *Chem. Soc. Rev.*, 2014, **43**, 744.

19 G. Xu, S. Zeng, B. Zhang, M. T. Swihart, K.-T. Yong and P. N. Prasad, *Chem. Rev.*, 2016, **116**, 12234.

20 A. Privitera, M. Righetto, F. Cacialli and M. K. Riede, *Adv. Opt. Mater.*, 2021, **9**, 2100215.

21 M. J. Crane, L. M. Jacoby, T. A. Cohen, Y. Huang, C. K. Luscombe and D. R. Gamelin, *Nano Lett.*, 2020, **20**, 8626.

22 Z. Wu, Y. Zhang, R. Hu, M. Jiang, P. Liang, Q. Yang, L. Deng, T. Jia, Z. Sun and D. Feng, *J. Phys. Chem. Lett.*, 2021, **12**, 2126.

23 Z. Luo, S. Sun, A. Karasahin, A. S. Bracker, S. G. Carter, M. K. Yakes, D. Gammon and E. Waks, *Nano Lett.*, 2019, **19**, 7072.

24 Y.-J. Wei, Y.-M. He, M.-C. Chen, Y.-N. Hu, Y. He, D. Wu, C. Schneider, M. Kamp, S. Höfling, C.-Y. Lu and J.-W. Pan, *Nano Lett.*, 2014, **14**, 6515.

25 G. Zorn, S. R. Dave, T. Weidner, X. Gao and D. G. Castner, *Surf. Sci.*, 2016, **648**, 339.

26 K. G. Crawford, I. Maini, D. A. Macdonald and D. A. J. Moran, *Prog. Surf. Sci.*, 2021, **96**, 100613.

27 M. I. Landstrass and K. V. Ravi, *Appl. Phys. Lett.*, 1989, **55**, 975.

28 J. A. Garrido, S. Nowy, A. Härtl and M. Stutzmann, *Langmuir*, 2008, **24**, 3897.

29 M. V. Hauf, B. Grotz, B. Naydenov, M. Dankerl, S. Pezzagna, J. Meijer, F. Jelezko, J. Wrachtrup, M. Stutzmann, F. Reinhard and J. A. Garrido, *Phys. Rev. B: Condens. Matter Mater. Phys.*, 2011, **83**, 081304.

30 P. R. Brown, D. Kim, R. R. Lunt, N. Zhao, M. G. Bawendi, J. C. Grossman and V. Bulović, *ACS Nano*, 2014, **8**, 5863.

31 D. M. Kroupa, M. Vörös, N. P. Brawand, B. W. McNichols, E. M. Miller, J. Gu, A. J. Nozik, A. Sellinger, G. Galli and M. C. Beard, *Nat. Commun.*, 2017, **8**, 15257.

32 J. Raymakers, K. Haenen and W. Maes, *J. Mater. Chem. C*, 2019, **7**, 10134.

33 K. E. Sapsford, W. R. Algar, L. Berti, K. B. Gemmill, B. J. Casey, E. Oh, M. H. Stewart and I. L. Medintz, *Chem. Rev.*, 2013, **113**, 1904.

34 G. Palui, F. Aldeek, W. Wang and H. Mattoussi, *Chem. Soc. Rev.*, 2015, **44**, 193.

35 A. Heuer-Jungemann, N. Feliu, I. Bakaimi, M. Hamaly, A. Alkilany, I. Chakraborty, A. Masood, M. F. Casula, A. Kostopoulou, E. Oh, K. Susumu, M. H. Stewart, I. L. Medintz, E. Stratakis, W. J. Parak and A. G. Kanaras, *Chem. Rev.*, 2019, **119**, 4819.

36 L. Protesescu, S. Yakunin, M. I. Bodnarchuk, F. Krieg, R. Caputo, C. H. Hendon, R. X. Yang, A. Walsh and M. V. Kovalenko, *Nano Lett.*, 2015, **15**, 3692.

37 A. I. Ekimov, A. L. Efros and A. A. Onushchenko, *Solid State Commun.*, 1985, **56**, 921.

38 M. A. Boles, D. Ling, T. Hyeon and D. V. Talapin, *Nat. Mater.*, 2016, **15**, 141.

39 M. L. H. Green and G. Parkin, *J. Chem. Educ.*, 2014, **91**, 807.

40 R. Koole, P. Schapotschnikow, C. de Mello Donegá, T. J. H. Vlugt and A. Meijerink, *ACS Nano*, 2008, **2**, 1703.

41 N. C. Anderson, P. E. Chen, A. K. Buckley, J. D. Roo and J. S. Owen, *J. Am. Chem. Soc.*, 2018, **140**, 7199.

42 R. Dierick, F. Van den Broeck, K. De Nolf, Q. Zhao, A. Vantomme, J. C. Martins and Z. Hens, *Chem. Mater.*, 2014, **26**, 5950.

43 D. W. Houck and B. A. Korgel, *Chem. Mater.*, 2018, **30**, 8359.

44 Y. Zhou, F. Wang and W. E. Buhro, *J. Am. Chem. Soc.*, 2015, **137**, 15198.

45 K. N. Lawrence, P. Dutta, M. Nagaraju, M. B. Teunis, B. B. Muhoberac and R. Sardar, *J. Am. Chem. Soc.*, 2016, **138**, 12813.

46 N. C. Anderson, M. P. Hendricks, J. J. Choi and J. S. Owen, *J. Am. Chem. Soc.*, 2013, **135**, 18536.

47 J. Zhang, H. Zhang, W. Cao, Z. Pang, J. Li, Y. Shu, C. Zhu, X. Kong, L. Wang and X. Peng, *J. Am. Chem. Soc.*, 2019, **141**, 15675.

48 A. Ritchhart and B. M. Cossairt, *Inorg. Chem.*, 2019, **58**, 2840.

49 R. Gomes, A. Hassinen, A. Szczygiel, Q. Zhao, A. Vantomme, J. C. Martins and Z. Hens, *J. Phys. Chem. Lett.*, 2011, **2**, 145.

50 J. De Roo, F. Van den Broeck, K. De Keukeleere, J. C. Martins, I. Van Driessche and Z. Hens, *J. Am. Chem. Soc.*, 2014, **136**, 9650.

51 J. De Roo, Y. Justo, K. De Keukeleere, F. Van den Broeck, J. C. Martins, I. Van Driessche and Z. Hens, *Angew. Chem., Int. Ed.*, 2015, **54**, 6488.

52 C. Sun and J. C. Berg, *Adv. Colloid Interface Sci.*, 2003, **105**, 151.

53 A. Nag, M. V. Kovalenko, J.-S. Lee, W. Liu, B. Spokoyny and D. V. Talapin, *J. Am. Chem. Soc.*, 2011, **133**, 10612.

54 H. Häkkinen, *Nat. Chem.*, 2012, **4**, 443.

55 L. M. Rossi, J. L. Fiorio, M. A. S. Garcia and C. P. Ferraz, *Dalton Trans.*, 2018, **47**, 5889.

56 M. Y. Gee, Y. Shen and A. B. Greytak, *J. Phys. Chem. C*, 2020, **124**, 23964.

57 O. Elimelech, O. Aviv, M. Oded and U. Banin, *Nano Lett.*, 2020, **20**, 6396.

58 J. J. Calvin, E. A. O'Brien, A. B. Sedlak, A. D. Balan and A. P. Alivisatos, *ACS Nano*, 2021, **15**, 1407.

59 V. Ravi, J. M. Binz and R. M. Rioux, *Nano Lett.*, 2013, **13**, 4442.

60 C. K. Møller, *Nature*, 1958, **182**, 1436.

61 A. Kojima, K. Teshima, Y. Shirai and T. Miyasaka, *J. Am. Chem. Soc.*, 2009, **131**, 6050.

62 L. Etgar, P. Gao, Z. Xue, Q. Peng, A. K. Chandiran, B. Liu, M. K. Nazeeruddin and M. Grätzel, *J. Am. Chem. Soc.*, 2012, **134**, 17396.

63 M. M. Lee, J. Teuscher, T. Miyasaka, T. N. Murakami and H. J. Snaith, *Science*, 2012, **338**, 643.

64 D. P. McMeekin, Z. Wang, W. Rehman, F. Pulvirenti, J. B. Patel, N. K. Noel, M. B. Johnston, S. R. Marder, L. M. Herz and H. J. Snaith, *Adv. Mater.*, 2017, **29**, 1607039.

65 J. Berry, T. Buonassisi, D. A. Egger, G. Hodes, L. Kronik, Y.-L. Loo, I. Lubomirsky, S. R. Marder, Y. Mastai, J. S. Miller, D. B. Mitzi, Y. Paz, A. M. Rappe, I. Riess, B. Rybtchinski, O. Stafsudd, V. Stevanovic, M. F. Toney, D. Zitoun, A. Kahn, D. Ginley and D. Cahen, *Adv. Mater.*, 2015, **27**, 5102.

66 S. Song, R. Hill, K. Choi, K. Wojciechowski, S. Barlow, J. Leisen, H. J. Snaith, S. R. Marder and T. Park, *Nano Energy*, 2018, **49**, 324.

67 D. A. Valverde-Chávez, E. Rojas-Gatjens, J. Williamson, S. Jariwala, Y. Shi, D. P. McCarthy, S. Barlow, S. R. Marder, D. S. Ginger and C. Silva-Acuña, *J. Mater. Chem. C*, 2021, **9**, 8204.

68 J. Jeong, M. Kim, J. Seo, H. Lu, P. Ahlawat, A. Mishra, Y. Yang, M. A. Hope, F. T. Eickemeyer, M. Kim, Y. J. Yoon, I. W. Choi, B. P. Darwich, S. J. Choi, Y. Jo, J. H. Lee, B. Walker, S. M. Zakeeruddin, L. Emsley, U. Rothlisberger, A. Hagfeldt, D. S. Kim, M. Grätzel and J. Y. Kim, *Nature*, 2021, **592**, 381.

69 R. Lin, K. Xiao, Z. Qin, Q. Han, C. Zhang, M. Wei, M. I. Saidaminov, Y. Gao, J. Xu, M. Xiao, A. Li, J. Zhu, E. H. Sargent and H. Tan, *Nat. Energy*, 2019, **4**, 864.

70 A. Al-Ashouri, E. Köhnen, B. Li, A. Magomedov, H. Hempel, P. Caprioglio, J. A. Márquez, A. B. M. Vilches, E. Kasparavicius, J. A. Smith, N. Phung, D. Menzel, M. Grischek, L. Kegelmann, D. Skroblin, C. Gollwitzer, T. Malinauskas, M. Jošt, G. Matič, B. Rech, R. Schlatmann, M. Topič, L. Korte, A. Abate, B. Stannowski, D. Neher, M. Stolterfoht, T. Unold, V. Getautis and S. Albrecht, *Science*, 2020, **370**, 1300.

71 B. A. Koscher, J. K. Swabeck, N. D. Bronstein and A. P. Alivisatos, *J. Am. Chem. Soc.*, 2017, **139**, 6566.

72 Y. Zhang, T. D. Siegler, C. J. Thomas, M. K. Abney, T. Shah, A. De Gorostiza, R. M. Greene and B. A. Korgel, *Chem. Mater.*, 2020, **32**, 5410.

73 N. Pradhan, *ACS Energy Lett.*, 2019, **4**, 1634.

74 H. Utzat, K. E. Shulenberger, O. B. Achorn, M. Nasilowski, T. S. Sinclair and M. G. Bawendi, *Nano Lett.*, 2017, **17**, 6838.

75 Z. Chen, H. Li, Y. Tang, X. Huang, D. Ho and C.-S. Lee, *Mater. Res. Express*, 2014, **1**, 015034.

76 G. Li, Z.-K. Tan, D. Di, M. L. Lai, L. Jiang, J. H.-W. Lim, R. H. Friend and N. C. Greenham, *Nano Lett.*, 2015, **15**, 2640.

77 L. Zhao, K. Roh, S. Kacmoli, K. Al Kurdi, S. Jhulki, S. Barlow, S. R. Marder, C. Gmachl and B. P. Rand, *Adv. Mater.*, 2020, **32**, 2000752.

78 S. Yakunin, L. Protesescu, F. Krieg, M. I. Bodnarchuk, G. Nedelcu, M. Humer, G. D. Luca, M. Fiebig, W. Heiss and M. V. Kovalenko, *Nat. Commun.*, 2015, **6**, 8056.

79 Y. Jia, R. A. Kerner, A. J. Grede, A. N. Brigeman, B. P. Rand and N. C. Giebink, *Nano Lett.*, 2016, **16**, 4624.

80 Y. Jia, R. A. Kerner, A. J. Grede, B. P. Rand and N. C. Giebink, *Nat. Photonics*, 2017, **11**, 784.

81 H. Kim, K. Roh, J. P. Murphy, L. Zhao, W. B. Gunnarsson, E. Longhi, S. Barlow, S. R. Marder, B. P. Rand and N. C. Giebink, *Adv. Opt. Mater.*, 2020, **8**, 1901297.

82 H. Wei, Y. Fang, P. Mulligan, W. Chuirazzi, H.-H. Fang, C. Wang, B. R. Ecker, Y. Gao, M. A. Loi, L. Cao and J. Huang, *Nat. Photonics*, 2016, **10**, 333.

83 J. Liu, B. Shabbir, C. Wang, T. Wan, Q. Ou, P. Yu, A. Tadich, X. Jiao, D. Chu, D. Qi, D. Li, R. Kan, Y. Huang, Y. Dong, J. Jasieniak, Y. Zhang and Q. Bao, *Adv. Mater.*, 2019, **31**, 1901644.

84 T. A. Cohen, T. J. Milstein, D. M. Kroupa, J. D. MacKenzie, C. K. Luscombe and D. R. Gamelin, *J. Mater. Chem. A*, 2019, **7**, 9279.

85 X. Luo, T. Ding, X. Liu, Y. Liu and K. Wu, *Nano Lett.*, 2019, **19**, 338.

86 K. Nikolaidou, S. Sarang, C. Hoffman, B. Mendewala, H. Ishihara, J. Q. Lu, B. Ilan, V. Tung and S. Ghosh, *Adv. Opt. Mater.*, 2016, **4**, 2126.

87 J. Tong, J. Luo, L. Shi, J. Wu, L. Xu, J. Song, P. Wang, H. Li and Z. Deng, *J. Mater. Chem. A*, 2019, **7**, 4872.

88 F. Meinardi, Q. A. Akkerman, F. Bruni, S. Park, M. Mauri, Z. Dang, L. Manna and S. Brovelli, *ACS Energy Lett.*, 2017, **2**, 2368.

89 G. Rainò, G. Nedelcu, L. Protesescu, M. I. Bodnarchuk, M. V. Kovalenko, R. F. Mahrt and T. Stöferle, *ACS Nano*, 2016, **10**, 2485.

90 Y.-S. Park, S. Guo, N. S. Makarov and V. I. Klimov, *ACS Nano*, 2015, **9**, 10386.

91 H. Utzat, W. Sun, A. E. K. Kaplan, F. Krieg, M. Ginterseder, B. Spokoyny, N. D. Klein, K. E. Shulenberger, C. F. Perkinson, M. V. Kovalenko and M. G. Bawendi, *Science*, 2019, **363**, 1068.

92 Q. A. Akkerman, G. Rainò, M. V. Kovalenko and L. Manna, *Nat. Mater.*, 2018, **17**, 394.

93 D. P. Nenon, K. Pressler, J. Kang, B. A. Koscher, J. H. Olshansky, W. T. Osowiecki, M. A. Koc, L.-W. Wang and A. P. Alivisatos, *J. Am. Chem. Soc.*, 2018, **140**, 17760.

94 J. Kang and L.-W. Wang, *J. Phys. Chem. Lett.*, 2017, **8**, 489.

95 S. Ten Brinck, F. Zaccaria and I. Infante, *ACS Energy Lett.*, 2019, **4**, 2739.

96 S. E. Creutz, E. N. Crites, M. C. De Siena and D. R. Gamelin, *Chem. Mater.*, 2018, **30**, 4887.

97 G. Nedelcu, L. Protesescu, S. Yakunin, M. I. Bodnarchuk, M. J. Grotevent and M. V. Kovalenko, *Nano Lett.*, 2015, **15**, 5635.

98 M. Imran, V. Caligiuri, M. Wang, L. Goldoni, M. Prato, R. Krahne, L. De Trizio and L. Manna, *J. Am. Chem. Soc.*, 2018, **140**, 2656.

99 T. J. Milstein, D. M. Kroupa and D. R. Gamelin, *Nano Lett.*, 2018, **18**, 3792.

100 W. Liu, Q. Lin, H. Li, K. Wu, I. Robel, J. M. Pietryga and V. I. Klimov, *J. Am. Chem. Soc.*, 2016, **138**, 14954.

101 G. Pan, X. Bai, D. Yang, X. Chen, P. Jing, S. Qu, L. Zhang, D. Zhou, J. Zhu, W. Xu, B. Dong and H. Song, *Nano Lett.*, 2017, **17**, 8005.

102 D. Zhou, D. Liu, G. Pan, X. Chen, D. Li, W. Xu, X. Bai and H. Song, *Adv. Mater.*, 2017, **29**, 1704149.

103 M. C. De Siena, D. E. Sommer, S. E. Creutz, S. T. Dunham and D. R. Gamelin, *Chem. Mater.*, 2019, **31**, 7711.

104 B. Conings, J. Drijkoningen, N. Gauquelin, A. Babayigit, J. D'Haen, L. D'Olieslaeger, A. Ethirajan, J. Verbeeck, J. Manca, E. Mosconi, F. D. Angelis and H.-G. Boyen, *Adv. Energy Mater.*, 2015, **5**, 1500477.

105 C. Manspeaker, S. Venkatesan, A. Zakhidov and K. S. Martirosyan, *Curr. Opin. Chem. Eng.*, 2017, **15**, 1.

106 G. Rainò, A. Landuyt, F. Krieg, C. Bernasconi, S. T. Ochsenbein, D. N. Dirin, M. I. Bodnarchuk and M. V. Kovalenko, *Nano Lett.*, 2019, **19**, 3648.

107 G. Yuan, C. Ritchie, M. Ritter, S. Murphy, D. E. Gómez and P. Mulvaney, *J. Phys. Chem. C*, 2018, **122**, 13407.

108 Y. Ogomi, A. Morita, S. Tsukamoto, T. Saitho, Q. Shen, T. Toyoda, K. Yoshino, S. S. Pandey, T. Ma and S. Hayase, *J. Phys. Chem. C*, 2014, **118**, 16651.

109 L. Zuo, Z. Gu, T. Ye, W. Fu, G. Wu, H. Li and H. Chen, *J. Am. Chem. Soc.*, 2015, **137**, 2674.

110 A. Pan, B. He, X. Fan, Z. Liu, J. J. Urban, A. P. Alivisatos, L. He and Y. Liu, *ACS Nano*, 2016, **10**, 7943.

111 V. K. Ravi, P. K. Santra, N. Joshi, J. Chugh, S. K. Singh, H. Rensmo, P. Ghosh and A. Nag, *J. Phys. Chem. Lett.*, 2017, **8**, 4988.

112 Z. Hens and J. C. Martins, *Chem. Mater.*, 2013, **25**, 1211.

113 S. ten Brinck and I. Infante, *ACS Energy Lett.*, 2016, **1**, 1266.

114 M. Imran, P. Ijaz, D. Baranov, L. Goldoni, U. Petralanda, Q. Akkerman, A. L. Abdelhady, M. Prato, P. Bianchini, I. Infante and L. Manna, *Nano Lett.*, 2018, **18**, 7822.

115 F. Krieg, S. T. Ochsenbein, S. Yakunin, S. ten Brinck, P. Aellen, A. Süess, B. Clerc, D. Guggisberg, O. Nazarenko, Y. Shynkarenko, S. Kumar, C.-J. Shih, I. Infante and M. V. Kovalenko, *ACS Energy Lett.*, 2018, **3**, 641.

116 Y. Cai, H. Wang, Y. Li, L. Wang, X. Lv, X. Yang and R.-J. Xie, *Chem. Mater.*, 2019, **31**, 881.

117 S. E. Creutz, E. N. Crites, M. C. De Siena and D. R. Gamelin, *Nano Lett.*, 2018, **18**, 1118.

118 D. Yoo, J. Y. Woo, Y. Kim, S. W. Kim, S.-H. Wei, S. Jeong and Y.-H. Kim, *J. Phys. Chem. Lett.*, 2020, **11**, 652.

119 F. Di Stasio, S. Christodoulou, N. Huo and G. Konstantatos, *Chem. Mater.*, 2017, **29**, 7663.

120 M. Imran, P. Ijaz, L. Goldoni, D. Maggioni, U. Petralanda, M. Prato, G. Almeida, I. Infante and L. Manna, *ACS Energy Lett.*, 2019, **4**, 819.

121 M. I. Bodnarchuk, S. C. Boehme, S. ten Brinck, C. Bernasconi, Y. Shynkarenko, F. Krieg, R. Widmer, B. Aeschlimann, D. Günther, M. V. Kovalenko and I. Infante, *ACS Energy Lett.*, 2019, **4**, 63.

122 A. Dutta, R. K. Behera, S. K. Dutta, S. Das Adhikari and N. Pradhan, *J. Phys. Chem. Lett.*, 2018, **9**, 6599.

123 H. Sun, Z. Yang, M. Wei, W. Sun, X. Li, S. Ye, Y. Zhao, H. Tan, E. L. Kynaston, T. B. Schon, H. Yan, Z.-H. Lu, G. A. Ozin, E. H. Sargent and D. S. Seferos, *Adv. Mater.*, 2017, **29**, 1701153.

124 S. Yakunin, J. Chaaban, B. M. Benin, I. Cherniukh, C. Bernasconi, A. Landuyt, Y. Shynkarenko, S. Bolat, C. Hofer, Y. E. Romanyuk, S. Cattaneo, S. I. Pokutnyi, R. D. Schaller, M. I. Bodnarchuk, D. Poulikakos and M. V. Kovalenko, *Nat. Commun.*, 2021, **12**, 981.

125 I. Cherniukh, G. Rainò, T. Stöferle, M. Burian, A. Travesset, D. Naumenko, H. Amenitsch, R. Erni, R. F. Mahrt, M. I. Bodnarchuk and M. V. Kovalenko, *Nature*, 2021, **593**, 535.

126 X. Li, M. Ibrahim Dar, C. Yi, J. Luo, M. Tschumi, S. M. Zakeeruddin, M. K. Nazeeruddin, H. Han and M. Grätzel, *Nat. Chem.*, 2015, **7**, 703.

127 D. W. deQuilettes, S. Koch, S. Burke, R. K. Paranji, A. J. Shropshire, M. E. Ziffer and D. S. Ginger, *ACS Energy Lett.*, 2016, **1**, 438.

128 F. Liu, Y. Zhang, C. Ding, S. Kobayashi, T. Izuishi, N. Nakazawa, T. Toyoda, T. Ohta, S. Hayase, T. Minemoto, K. Yoshino, S. Dai and Q. Shen, *ACS Nano*, 2017, **11**, 10373.

129 L. Wu, Q. Zhong, D. Yang, M. Chen, H. Hu, Q. Pan, H. Liu, M. Cao, Y. Xu, B. Sun and Q. Zhang, *Langmuir*, 2017, **33**, 12689.

130 H. Wang, N. Sui, X. Bai, Y. Zhang, Q. Rice, F. J. Seo, Q. Zhang, V. L. Colvin and W. W. Yu, *J. Phys. Chem. Lett.*, 2018, **9**, 4166.

131 H. Wang, X. Zhang, N. Sui, Y. Hu, V. L. Colvin, W. W. Yu and Y. Zhang, *ACS Appl. Mater. Interfaces*, 2020, **12**, 11769.

132 Y. Tan, Y. Zou, L. Wu, Q. Huang, D. Yang, M. Chen, M. Ban, C. Wu, T. Wu, S. Bai, T. Song, Q. Zhang and B. Sun, *ACS Appl. Mater. Interfaces*, 2018, **10**, 3784.

133 N. K. Noel, A. Abate, S. D. Stranks, E. S. Parrott, V. M. Burlakov, A. Goriely and H. J. Snaith, *ACS Nano*, 2014, **8**, 9815.

134 F. Krieg, Q. K. Ong, M. Burian, G. Rainò, D. Naumenko, H. Amenitsch, A. Süess, M. J. Grotevent, F. Krumeich, M. I. Bodnarchuk, I. Shorubalko, F. Stellacci and M. V. Kovalenko, *J. Am. Chem. Soc.*, 2019, **141**, 19839.

135 B. Zhang, L. Goldoni, J. Zito, Z. Dang, G. Almeida, F. Zaccaria, J. de Wit, I. Infante, L. De Trizio and L. Manna, *Chem. Mater.*, 2019, **31**, 9140.

136 B. Zhang, L. Goldoni, C. Lambruschini, L. Moni, M. Imran, A. Pianetti, V. Pinchetti, S. Brovelli, L. De Trizio and L. Manna, *Nano Lett.*, 2020, **20**, 8847.

137 Y. Shynkarenko, M. I. Bodnarchuk, C. Bernasconi, Y. Berezovska, V. Verteletskyi, S. T. Ochsenbein and M. V. Kovalenko, *ACS Energy Lett.*, 2019, **4**, 2703.

138 E. Mosconi, C. Quarti, T. Ivanovska, G. Ruani and F. D. Angelis, *Phys. Chem. Chem. Phys.*, 2014, **16**, 16137.

139 S. Liu, F. Zheng, N. Z. Koocher, H. Takenaka, F. Wang and A. M. Rappe, *J. Phys. Chem. Lett.*, 2015, **6**, 693.

140 A. Amat, E. Mosconi, E. Ronca, C. Quarti, P. Umari, M. K. Nazeeruddin, M. Grätzel and F. De Angelis, *Nano Lett.*, 2014, **14**, 3608.

141 S. Toyoshima, K. Kuwabara, T. Sakurai, T. Taima, K. Saito, H. Kato and K. Akimoto, *Jpn. J. Appl. Phys.*, 2007, **46**, 2692.

142 Y. R. Park, S. Eom, H. H. Kim, W. K. Choi and Y. Kang, *Sci. Rep.*, 2020, **10**, 14758.

143 M. Li, Y. Zhang, H. Gao, Y. Peng, S. Tang, L. Yu, R. Chen and W. Huang, *J. Phys. Chem. C*, 2021, **125**, 2866.

144 M.-S. Lee, S. Sarwar, S. Park, U. Asmat, D. T. Thuy, C.-H. Han, S. Ahn, I. Jeong and S. Hong, *Sustainable Energy Fuels*, 2020, **4**, 3318.

145 A. Bitar, N. M. Ahmad, H. Fessi and A. Elaissari, *Drug Discovery Today*, 2012, **17**, 1147.

146 S. T. Selvan, T. T. Tan and J. Y. Ying, *Adv. Mater.*, 2005, **17**, 1620.

147 J. Fokkema, J. Fermie, N. Liv, D. J. van den Heuvel, T. O. M. Konings, G. A. Blab, A. Meijerink, J. Klumperman and H. C. Gerritsen, *Sci. Rep.*, 2018, **8**, 13625.

148 Y. Xu, Y. Lv, R. Wu, J. Li, H. Shen, H. Yang, H. Zhang and L. S. Li, *Inorg. Chem.*, 2021, **60**, 6503.

149 L. M. Liz-Marzán, M. Giersig and P. Mulvaney, *Langmuir*, 1996, **12**, 4329.

150 Y. Han, Z. Lu, Z. Teng, J. Liang, Z. Guo, D. Wang, M.-Y. Han and W. Yang, *Langmuir*, 2017, **33**, 5879.

151 Y. Yang, L. Jing, X. Yu, D. Yan and M. Gao, *Chem. Mater.*, 2007, **19**, 4123.

152 Y. Han, J. Jiang, S. S. Lee and J. Y. Ying, *Langmuir*, 2008, **24**, 5842.

153 A. Guerrero-Martínez, J. Pérez-Juste and L. M. Liz-Marzán, *Adv. Mater.*, 2010, **22**, 1182.

154 S. Liu and M.-Y. Han, *Chem. – Asian J.*, 2010, **5**, 36.

155 S. T. Selvan, *Biointerphases*, 2010, **5**, FA110.

156 L. Lei, X. Liu, Y. Li, Y. Cui, Y. Yang and G. Qin, *Mater. Chem. Phys.*, 2011, **125**, 866.

157 I. V. Melnyk, R. P. Pogorilyi, Y. L. Zub, M. Vaclavikova, K. Gdula, A. Dąbrowski, G. A. Seisenbaeva and V. G. Kessler, *Sci. Rep.*, 2018, **8**, 8592.

158 M. J. Marchant, L. Guzmán, A. H. Corvalán and M. J. Kogan, *Nanomaterials*, 2019, **9**, 1333.

159 F. Heidari, M. Hekmati and H. Veisi, *J. Colloid Interface Sci.*, 2017, **501**, 175.

160 K.-M. Hsieh, K.-C. Lan, W.-L. Hu, M.-K. Chen, L.-S. Jang and M.-H. Wang, *Biosens. Bioelectron.*, 2013, **49**, 450.

161 J. V. Hollingsworth, N. V. S. D. K. Bhupathiraju, J. Sun, E. Lochner, M. G. H. Vicente and P. S. Russo, *ACS Appl. Mater. Interfaces*, 2016, **8**, 792.

162 M. Masteri-Farahani and S. Shahsavarifar, *Appl. Organomet. Chem.*, 2018, **32**, 4064.

163 R. Riedel, N. Mahr, C. Yao, A. Wu, F. Yang and N. Hampp, *Nanoscale*, 2020, **12**, 3007.

164 X. Hu and X. Gao, *ACS Nano*, 2010, **4**, 6080.

165 R. Koole, M. M. van Schooneveld, J. Hilhorst, K. Castermans, D. P. Cormode, G. J. Strijkers, C. de Mello Donegá, D. Vanmaekelbergh, A. W. Griffioen, K. Nicolay, Z. A. Fayad, A. Meijerink and W. J. M. Mulder, *Bioconjugate Chem.*, 2008, **19**, 2471.

166 M. M. van Schooneveld, A. Gloter, O. Stephan, L. F. Zagonel, R. Koole, A. Meijerink, W. J. M. Mulder and F. M. F. de Groot, *Nat. Nanotechnol.*, 2010, **5**, 538.

167 L. Mangolini, *J. Vac. Sci. Technol., B*, 2013, **31**, 020801.

168 V. N. Mochalin, O. Shenderova, D. Ho and Y. Gogotsi, *Nat. Nanotechnol.*, 2012, **7**, 11.

169 T.-W. Kim, C.-H. Cho, B.-H. Kim and S.-J. Park, *Appl. Phys. Lett.*, 2006, **88**, 123102.

170 S. P. Pujari, H. Driss, F. Bannani, B. van Lagen and H. Zuilhof, *Chem. Mater.*, 2018, **30**, 6503.

171 X. Zhang, D. Neiner, S. Wang, A. Y. Louie and S. M. Kauzlarich, *Nanotechnology*, 2007, **18**, 095601.

172 S. Xun, X. Song, L. Wang, M. E. Grass, Z. Liu, V. S. Battaglia and G. Liu, *J. Electrochem. Soc.*, 2011, **158**, A1260.

173 B. J. Winters, J. Holm and J. T. Roberts, *J. Nanopart. Res.*, 2011, **13**, 5473.

174 O. O. Mykhaylyk, Y. M. Solonin, D. N. Batchelder and R. Brydson, *J. Appl. Phys.*, 2005, **97**, 074302.

175 J. Xiao, G. Ouyang, P. Liu, C. X. Wang and G. W. Yang, *Nano Lett.*, 2014, **14**, 3645.

176 K. Iakoubovskii, M. V. Baidakova, B. H. Wouters, A. Stesmans, G. J. Adriaenssens, A. Y. Vul and P. J. Grobet, *Diamond Relat. Mater.*, 2000, **9**, 861.

177 K. M. Song, J. Y. Shim and H. K. Baik, *Diamond Relat. Mater.*, 2002, **11**, 185.

178 Z. Q. Li and Y. Zhou, *Phys. B*, 2010, **405**, 1004.

179 K. Niwase, T. Tanaka, Y. Kakimoto, K. N. Ishihara and P. H. Shingu, *Mater. Trans., JIM*, 1995, **36**, 282.

180 V. Pichot, M. Comet, E. Fousson, C. Baras, A. Senger, F. Le Normand and D. Spitzer, *Diamond Relat. Mater.*, 2008, **17**, 13.

181 C. L. Cheng, H. C. Chang, J. C. Lin, K. J. Song and J. K. Wang, *Phys. Rev. Lett.*, 1997, **78**, 3713.

182 P. Thissen, O. Seitz and Y. J. Chabal, *Prog. Surf. Sci.*, 2012, **87**, 272.

183 T. J. Barnes, K. L. Jarvis and C. A. Prestidge, *Ther. Delivery*, 2013, **4**, 811.

184 D. H. Jariwala, D. Patel and S. Wairkar, *Mater. Sci. Eng., C*, 2020, **113**, 110996.

185 N. Aissaoui, L. Bergaoui, J. Landoulsi, J.-F. Lambert and S. Boujday, *Langmuir*, 2012, **28**, 656.

186 X. Li, J. Shao, Y. Qin, C. Shao, T. Zheng and L. Ye, *J. Mater. Chem.*, 2011, **21**, 7966.

187 J. Hwang, M. P. Hwang, M. Choi, Y. Seo, Y. Jo, J. Son, J. Hong and J. Choi, *Sci. Rep.*, 2016, **6**, 35565.

188 I. S. Curtis, R. J. Wills and M. Dasog, *Nanoscale*, 2021, **13**, 2685.

189 Z. Kang, Y. Liu and S.-T. Lee, *Nanoscale*, 2011, **3**, 777.

190 J. B. Zang, Y. H. Wang, S. Z. Zhao, L. Y. Bian and J. Lu, *Diamond Relat. Mater.*, 2007, **16**, 16.

191 S. Jiang, B. Hu, R. Sahore, L. Zhang, H. Liu, L. Zhang, W. Lu, B. Zhao and Z. Zhang, *ACS Appl. Mater. Interfaces*, 2018, **10**, 44924.

192 M. J. Rutter and J. Robertson, *Phys. Rev. B: Condens. Matter Mater. Phys.*, 1998, **57**, 9241.

193 D. Mizuno, K. Yamasue and Y. Cho, *Appl. Phys. Lett.*, 2013, **103**, 101601.

194 V. Puddu and C. C. Perry, *ACS Nano*, 2012, **6**, 6356.

195 H. A. Girard, S. Perruchas, C. Gesset, M. Chaigneau, L. Vieille, J.-C. Arnault, P. Bergonzo, J.-P. Boilot and T. Gacoin, *ACS Appl. Mater. Interfaces*, 2009, **1**, 2738.

196 S. Ciampi, J. B. Harper and J. J. Gooding, *Chem. Soc. Rev.*, 2010, **39**, 2158.

197 E. G. Robins, M. P. Stewart and J. M. Buriak, *Chem. Commun.*, 1999, 2479.

198 B. Arkles, J. R. Steinmetz, J. Zazyczny and P. Mehta, *J. Adhes. Sci. Technol.*, 1992, **6**, 193.

199 A. Mesnage, X. Lefèvre, P. Jégou, G. Deniau and S. Palacin, *Langmuir*, 2012, **28**, 11767.

200 M. Busson, A. Berisha, C. Combellas, F. Kanoufi and J. Pinson, *Chem. Commun.*, 2011, **47**, 12631.

201 C.-H. Jung, K.-H. Kim and S.-H. Hong, *ACS Appl. Mater. Interfaces*, 2019, **11**, 26753.

202 Y. Zhang, A. A. Tamijani, M. E. Taylor, B. Zhi, C. L. Haynes, S. E. Mason and R. J. Hamers, *J. Am. Chem. Soc.*, 2019, **141**, 8277.

203 L. Diederich, O. M. Küttel, P. Aebi and L. Schlapbach, *Surf. Sci.*, 1998, **418**, 219.

204 L. A. Huck and J. M. Buriak, *Langmuir*, 2012, **28**, 16285.

205 J. P. L. Perez, J. Yu, A. J. Sheppard, S. D. Chambreau, G. L. Vaghjiani and S. L. Anderson, *ACS Appl. Mater. Interfaces*, 2015, **7**, 9991.

206 E. Fok, M. Shih, A. Meldrum and J. G. C. Veinot, *Chem. Commun.*, 2004, 386.

207 S. Gabriel, R. Jérôme and C. Jérôme, *Prog. Polym. Sci.*, 2010, **35**, 113.

208 E. V. Rogozhina, D. A. Eckhoff, E. Gratton and P. V. Braun, *J. Mater. Chem.*, 2006, **16**, 1421.

209 C. Stavis, T. L. Clare, J. E. Butler, A. D. Radadia, R. Carr, H. Zeng, W. P. King, J. A. Carlisle, A. Aksimentiev, R. Bashir and R. J. Hamers, *Proc. Natl. Acad. Sci. U. S. A.*, 2011, **108**, 983.

210 P. E. Colavita, B. Sun, K.-Y. Tse and R. J. Hamers, *J. Am. Chem. Soc.*, 2007, **129**, 13554.

211 C. Gautier, I. López and T. Breton, *Mater. Adv.*, 2021, **2**, 2773.

212 K. Brymora, J. Fouineau, A. Eddarir, F. Chau, N. Yaacoub, J.-M. Grenèche, J. Pinson, S. Ammar and F. Calvayrac, *J. Nanopart. Res.*, 2015, **17**, 438.

213 S. Betelu, I. Tijunelyte, L. Boubekeur-Lecaque, I. Ignatiadis, J. Ibrahim, S. Gaboreau, C. Berho, T. Toury, E. Guenin, N. Lidgi-Guigui, N. Félidj, E. Rinnert and M. L. D. L. Chapelle, *J. Phys. Chem. C*, 2016, **120**, 18158.

214 L. Laurentius, S. R. Stoyanov, S. Gusarov, A. Kovalenko, R. Du, G. P. Lopinski and M. T. McDermott, *ACS Nano*, 2011, **5**, 4219.

215 F. Mousli, A. Chaouchi, S. Hocine, A. Lamouri, M. Rei Vilar, A. Kadri and M. M. Chehimi, *Appl. Surf. Sci.*, 2019, **465**, 1078.

216 D. Hetemi, V. Noël and J. Pinson, *Biosensors*, 2020, **10**, 4.

217 N. Bondon, L. Raehm, C. Charnay, R. Boukherroub and J.-O. Durand, *J. Mater. Chem. B*, 2020, **8**, 10878.

218 A. Azioune, A. Ben Slimane, L. Ait Hamou, A. Pleuvy, M. M. Chehimi, C. Perruchot and S. P. Armes, *Langmuir*, 2004, **20**, 3350.

219 H.-H. Cho, H. Yang, D. J. Kang and B. J. Kim, *ACS Appl. Mater. Interfaces*, 2015, **7**, 8615.

220 L. Qian, Y. Zheng, J. Xue and P. H. Holloway, *Nat. Photonics*, 2011, **5**, 543.

221 W. Zhou, Y. Shang, F. P. García de Arquer, K. Xu, R. Wang, S. Luo, X. Xiao, X. Zhou, R. Huang, E. H. Sargent and Z. Ning, *Nat. Electron.*, 2020, **3**, 251.

222 A. Kiani, B. R. Sutherland, Y. Kim, O. Ouellette, L. Levina, G. Walters, C.-T. Dinh, M. Liu, O. Voznyy, X. Lan, A. J. Labelle, A. H. Ip, A. Proppe, G. H. Ahmed, O. F. Mohammed, S. Hoogland and E. H. Sargent, *Appl. Phys. Lett.*, 2016, **109**, 183105.

223 R. Schmid, *Monatsh. Chem.*, 2001, **132**, 1295.

224 Q. Lu, C. Wu, D. Liu, H. Wang, W. Su, H. Li, Y. Zhang and S. Yao, *Green Chem.*, 2017, **19**, 900.

225 T. A. Cohen, Y. Huang, N. A. Bricker, C. S. Juhl, T. J. Milstein, J. D. MacKenzie, C. K. Luscombe and D. R. Gamelin, *Chem. Mater.*, 2021, **33**, 3779.

226 S. Wang, L. Du, Z. Jin, Y. Xin and H. Mattoussi, *J. Am. Chem. Soc.*, 2020, **142**, 12669.

227 B. Shi, J. Lü, Y. Liu, Y. Xiao and C. Lü, *Mater. Chem. Front.*, 2021, **5**, 4343.

228 S. M. Lee, H. Jung, W. I. Park, Y. Lee, E. Koo and J. Bang, *ChemistrySelect*, 2018, **3**, 11320.

229 J. Liu, T. Tanaka, K. Sivula, A. P. Alivisatos and J. M. J. Fréchet, *J. Am. Chem. Soc.*, 2004, **126**, 6550.

230 E. T. Vickers, T. A. Graham, A. H. Chowdhury, B. Bahrami, B. W. Dreskin, S. Lindley, S. B. Naghadeh, Q. Qiao and J. Z. Zhang, *ACS Energy Lett.*, 2018, **3**, 2931.

231 D. Cui, J. Xu, T. Zhu, G. Paradee, S. Ashok and M. Gerhold, *Appl. Phys. Lett.*, 2006, **88**, 183111.

232 Y. Liu, S. R. Scully, M. D. McGehee, J. Liu, C. K. Luscombe, J. M. J. Fréchet, S. E. Shaheen and D. S. Ginley, *J. Phys. Chem. B*, 2006, **110**, 3257.

233 C. Goh, S. R. Scully and M. D. McGehee, *J. Appl. Phys.*, 2007, **101**, 114503.

234 A. E. Colbert, W. Wu, E. M. Janke, F. Ma and D. S. Ginger, *J. Phys. Chem. C*, 2015, **119**, 24733.

235 J. Park, J. H. Lee, H. Doh, S. W. Heo, K. Cho, S. Kim, S. Cho and J. Bang, *J. Phys. Chem. C*, 2020, **124**, 25775.

236 Z. Yang, J. Z. Fan, A. H. Proppe, F. P. G. D. Arquer, D. Rossouw, O. Voznyy, X. Lan, M. Liu, G. Walters, R. Quintero-Bermudez, B. Sun, S. Hoogland, G. A. Botton, S. O. Kelley and E. H. Sargent, *Nat. Commun.*, 2017, **8**, 1325.

237 H. Zhang, J. Jang, W. Liu and D. V. Talapin, *ACS Nano*, 2014, **8**, 7359.

238 M.-J. Choi, F. P. García de Arquer, A. H. Proppe, A. Seifitokaldani, J. Choi, J. Kim, S.-W. Baek, M. Liu, B. Sun, M. Biondi, B. Scheffel, G. Walters, D.-H. Nam, J. W. Jo, O. Ouellette, O. Voznyy, S. Hoogland, S. O. Kelley, Y. S. Jung and E. H. Sargent, *Nat. Commun.*, 2020, **11**, 103.

239 R. A. Marcus, *J. Chem. Phys.*, 1956, **24**, 966.

240 K. E. Knowles, M. D. Peterson, M. R. McPhail and E. A. Weiss, *J. Phys. Chem. C*, 2013, **117**, 10229.

241 C. Yun, J. Lee, J. Lee, B. Lüssem, F. Ventsch, K. Leo and M. C. Gather, *Appl. Phys. Lett.*, 2012, **101**, 243303.

242 B. Minaev, G. Baryshnikov and H. Agren, *Phys. Chem. Chem. Phys.*, 2014, **16**, 1719.

243 Y. Huang, D. L. Elder, A. L. Kwiram, S. A. Jenekhe, A. K. Y. Jen, L. R. Dalton and C. K. Luscombe, *Adv. Mater.*, 2021, **33**, 1904239.

244 Y.-J. Cheng, S.-H. Yang and C.-S. Hsu, *Chem. Rev.*, 2009, **109**, 5868.

245 Y. Huang, T. A. Cohen, P. J. W. Sommerville and C. K. Luscombe, *J. Mater. Chem. C*, 2021, **9**, 7274.

246 Y. Hassan, T. Janes, R. D. Pensack, S. Rafiq, P. M. Brodersen, M. A. Winnik, D. Song and G. D. Scholes, *Chem. Mater.*, 2016, **28**, 4953.

247 K. Tarafder, Y. Surendranath, J. H. Olshansky, A. P. Alivisatos and L.-W. Wang, *J. Am. Chem. Soc.*, 2014, **136**, 5121.

248 J. H. Olshansky, A. D. Balan, T. X. Ding, X. Fu, Y. V. Lee and A. P. Alivisatos, *ACS Nano*, 2017, **11**, 8346.

249 J. H. Olshansky, T. X. Ding, Y. V. Lee, S. R. Leone and A. P. Alivisatos, *J. Am. Chem. Soc.*, 2015, **137**, 15567.

250 J. Huang, K. L. Mulfort, P. Du and L. X. Chen, *J. Am. Chem. Soc.*, 2012, **134**, 16472.

251 A. J. Morris-Cohen, M. T. Frederick, L. C. Cass and E. A. Weiss, *J. Am. Chem. Soc.*, 2011, **133**, 10146.

252 A. J. Harvie, C. T. Smith, R. Ahumada-Lazo, L. J. C. Jeuken, M. Califano, R. S. Bon, S. J. O. Hardman, D. J. Binks and K. Critchley, *J. Phys. Chem. C*, 2018, **122**, 10173.

253 H. Zhao, C. Sun, H. Yin, Y. Li, J. Gao, Y. Shi and M. Sun, *Sci. Rep.*, 2019, **9**, 7756.

254 D. A. Henckel, M. J. Enright, N. Panahpour Eslami, D. M. Kroupa, D. R. Gamelin and B. M. Cossairt, *Nano Lett.*, 2020, **20**, 2620.

255 E. P. A. M. Bakkers, A. W. Marsman, L. W. Jenneskens and D. Vanmaekelbergh, *Angew. Chem., Int. Ed.*, 2000, **39**, 2297.

256 R. S. Dibbell and D. F. Watson, *J. Phys. Chem. C*, 2009, **113**, 3139.

257 A. J. Morris-Cohen, M. D. Peterson, M. T. Frederick, J. M. Kamm and E. A. Weiss, *J. Phys. Chem. Lett.*, 2012, **3**, 2840.

258 J. J. Buckley, E. Couderc, M. J. Greaney, J. Munteanu, C. T. Riche, S. E. Bradforth and R. L. Brutchey, *ACS Nano*, 2014, **8**, 2512.

259 L. Stryer and R. P. Haugland, *Proc. Natl. Acad. Sci. U. S. A.*, 1967, **58**, 719.

260 B. Schuler, *Chem. Phys. Chem.*, 2005, **6**, 1206.

261 T. Förster, *Ann. Phys.*, 1948, **437**, 55.

262 I. L. Medintz and H. Mattoussi, *Phys. Chem. Chem. Phys.*, 2009, **11**, 17.

263 C. Mongin, S. Garakyaraghi, N. Razgoniaeva, M. Zamkov and F. N. Castellano, *Science*, 2016, **351**, 369.

264 Z. Huang and M. L. Tang, *J. Am. Chem. Soc.*, 2017, **139**, 9412.

265 Z.-W. Xi, L. Yang, D.-Y. Wang, C.-W. Feng, Y. Qin, Y.-M. Shen, C. Pu and X. Peng, *J. Org. Chem.*, 2021, **86**, 2474.

266 M. J. Enright, K. Gilbert-Bass, H. Sarsito and B. M. Cossairt, *Chem. Mater.*, 2019, **31**, 2677.

267 J. A. Caputo, L. C. Frenette, N. Zhao, K. L. Sowers, T. D. Krauss and D. J. Weix, *J. Am. Chem. Soc.*, 2017, **139**, 4250.

268 M. Zhang, Z. Li, X. Xin, J. Zhang, Y. Feng and H. Lv, *ACS Catal.*, 2020, **10**, 14793.

269 Y. Sahin, A. T. Sika-Nartey, K. E. Ercan, Y. Kocak, S. Senol, E. Ozensoy and Y. E. Türkmen, *ACS Appl. Mater. Interfaces*, 2021, **13**, 5099.

270 X. Zhu, Y. Lin, Y. Sun, M. C. Beard and Y. Yan, *J. Am. Chem. Soc.*, 2019, **141**, 733.

271 H. Xu, S. Ouyang, L. Liu, P. Reunchan, N. Umezawa and J. Ye, *J. Mater. Chem. A*, 2014, **2**, 12642.

272 C. B. Ong, L. Y. Ng and A. W. Mohammad, *Renewable Sustainable Energy Rev.*, 2018, **81**, 536.

273 Y. Huang, Z. Liu, G. Gao, Q. Xiao, W. Martens, A. Du, S. Sarina, C. Guo and H. Zhu, *Catal. Sci. Technol.*, 2018, **8**, 726.

274 U. Aslam, V. G. Rao, S. Chavez and S. Linic, *Nat. Catal.*, 2018, **1**, 656.

275 J. Bang, S. Das, E.-J. Yu, K. Kim, H. Lim, S. Kim and J. W. Hong, *Nano Lett.*, 2020, **20**, 6263.

276 A. Meng, B. Zhu, B. Zhong, L. Zhang and B. Cheng, *Appl. Surf. Sci.*, 2017, **422**, 518.

277 Y. Yuan, H. Zhu, K. Hills-Kimball, T. Cai, W. Shi, Z. Wei, H. Yang, Y. Candler, P. Wang, J. He and O. Chen, *Angew. Chem., Int. Ed.*, 2020, **59**, 22563.

278 Z. Zhang, K. Edme, S. Lian and E. A. Weiss, *J. Am. Chem. Soc.*, 2017, **139**, 4246.

279 X. Wu, S. Xie, C. Liu, C. Zhou, J. Lin, J. Kang, Q. Zhang, Z. Wang and Y. Wang, *ACS Catal.*, 2019, **9**, 8443.

280 M. B. Wilker, J. K. Utterback, S. Greene, K. A. Brown, D. W. Mulder, P. W. King and G. Dukovic, *J. Phys. Chem. C*, 2018, **122**, 741.

281 S. Yu, X.-B. Fan, X. Wang, J. Li, Q. Zhang, A. Xia, S. Wei, L.-Z. Wu, Y. Zhou and G. R. Patzke, *Nat. Commun.*, 2018, **9**, 4009.

282 J. G. Smith and P. K. Jain, *J. Am. Chem. Soc.*, 2016, **138**, 6765.

283 E. H. Edwards, A. A. Fertig, K. P. McClelland, M. T. Meidenbauer, S. Chakraborty, T. D. Krauss, K. L. Bren and E. M. Matson, *Chem. Commun.*, 2020, **56**, 8762.

284 M. J. Berr, P. Wagner, S. Fischbach, A. Vaneski, J. Schneider, A. S. Susha, A. L. Rogach, F. Jäckel and J. Feldmann, *Appl. Phys. Lett.*, 2012, **100**, 223903.

285 R. Abargues, J. Navarro, P. J. Rodríguez-Cantó, A. Maulu, J. F. Sánchez-Royo and J. P. Martínez-Pastor, *Nanoscale*, 2019, **11**, 1978.

286 X.-B. Li, B. Liu, M. Wen, Y.-J. Gao, H.-L. Wu, M.-Y. Huang, Z.-J. Li, B. Chen, C.-H. Tung and L.-Z. Wu, *Adv. Sci.*, 2016, **3**, 1500282.

287 H. Lu, X. Zhu, C. Miller, J. San Martin, X. Chen, E. M. Miller, Y. Yan and M. C. Beard, *J. Chem. Phys.*, 2019, **151**, 204305.

288 C. M. Wolff, P. D. Frischmann, M. Schulze, B. J. Bohn, R. Wein, P. Livadas, M. T. Carlson, F. Jäckel, J. Feldmann, F. Würthner and J. K. Stolarczyk, *Nat. Energy*, 2018, **3**, 862.

289 Z. Chen, Y. Hu, J. Wang, Q. Shen, Y. Zhang, C. Ding, Y. Bai, G. Jiang, Z. Li and N. Gaponik, *Chem. Mater.*, 2020, **32**, 1517.

290 L. C. M. Souza, T. A. Santos, C. R. A. Do Prado, B. A. V. Lima, R. S. Corrêa, A. A. Batista, L. Otubo, J. Ellena, L. T. Ueno, L. R. Dinelli and A. L. Bogado, *RSC Adv.*, 2016, **6**, 53130.

291 Y. Jiang, C. Wang, C. R. Rogers, M. S. Kodaimati and E. A. Weiss, *Nat. Chem.*, 2019, **11**, 1034.

292 W. Li, J. R. Lee and F. Jäckel, *ACS Appl. Mater. Interfaces*, 2016, **8**, 29434.

293 K. P. Acharya, R. S. Khnayzer, T. O'Connor, G. Diederich, M. Kirsanova, A. Klinkova, D. Roth, E. Kinder, M. Imboden and M. Zamkov, *Nano Lett.*, 2011, **11**, 2919.

294 M. Melchionna and P. Fornasiero, *ACS Catal.*, 2020, **10**, 5493.

295 P. Christopher, S. Jin, K. Sivula and P. V. Kamat, *ACS Energy Lett.*, 2021, **6**, 707.

296 V. Kuznetsova, Y. Gromova, M. Martinez-Carmona, F. Purcell-Milton, E. Ushakova, S. Cherevkov, V. Maslov and Y. K. Gun'ko, *Nanophotonics*, 2021, **10**, 797.

297 A. Ben Moshe, D. Szwarcman and G. Markovich, *ACS Nano*, 2011, **5**, 9034.

298 U. Tohgha, K. K. Deol, A. G. Porter, S. G. Bartko, J. K. Choi, B. M. Leonard, K. Varga, J. Kubelka, G. Muller and M. Balaz, *ACS Nano*, 2013, 7, 11094.

299 J. K. Choi, B. E. Haynie, U. Tohgha, L. Pap, K. W. Elliott, B. M. Leonard, S. V. Dzyuba, K. Varga, J. Kubelka and M. Balaz, *ACS Nano*, 2016, **10**, 3809.

300 N. Suzuki, Y. Wang, P. Elvati, Z.-B. Qu, K. Kim, S. Jiang, E. Baumeister, J. Lee, B. Yeom, J. H. Bahng, J. Lee, A. Violi and N. A. Kotov, *ACS Nano*, 2016, **10**, 1744.

301 T. He, J. Li, X. Li, C. Ren, Y. Luo, F. Zhao, R. Chen, X. Lin and J. Zhang, *Appl. Phys. Lett.*, 2017, **111**, 151102.

302 C. Chen, L. Gao, W. Gao, C. Ge, X. Du, Z. Li, Y. Yang, G. Niu and J. Tang, *Nat. Commun.*, 2019, **10**, 1927.

303 A. Ben-Moshe, A. Teitelboim, D. Oron and G. Markovich, *Nano Lett.*, 2016, **16**, 7467.

304 H. Zhang, H. He, X. Jiang, Z. Xia and W. Wei, *ACS Appl. Mater. Interfaces*, 2018, **10**, 30680.

305 W. Ma, L. Xu, L. Wang, C. Xu and H. Kuang, *Adv. Funct. Mater.*, 2019, **29**, 1805512.

306 C. Hao, R. Gao, Y. Li, L. Xu, M. Sun, C. Xu and H. Kuang, *Angew. Chem., Int. Ed.*, 2019, **58**, 7371.

307 V. V. Belykh, D. R. Yakovlev, M. M. Glazov, P. S. Grigoryev, M. Hussain, J. Rautert, D. N. Dirin, M. V. Kovalenko and M. Bayer, *Nat. Commun.*, 2019, **10**, 1.

308 K. Trujillo-Hernández, G. Rodríguez-López, A. Espinosa-Roa, J. González-Roque, A. P. Gómora-Figueroa, W. Zhang, P. S. Halasyamani, V. Jancik, M. Gembicky, G. Pirruccio and D. Solis-Ibarra, *J. Mater. Chem. C*, 2020, **8**, 9602.

309 Y.-H. Kim, Y. Zhai, H. Lu, X. Pan, C. Xiao, E. A. Gaulding, S. P. Harvey, J. J. Berry, Z. V. Vardeny, J. M. Luther and M. C. Beard, *Science*, 2021, **371**, 1129.

310 K. E. Sapsford, T. Pons, I. L. Medintz, S. Higashiya, F. M. Brunel, P. E. Dawson and H. Mattoussi, *J. Phys. Chem. C*, 2007, **111**, 11528.

311 J. Wang, P. Jiang, Z. Han, L. Qiu, C. Wang, B. Zheng and J. Xia, *Langmuir*, 2012, **28**, 7962.

312 Y. Cui, S. N. Kim, S. E. Jones, L. L. Wissler, R. R. Naik and M. C. McAlpine, *Nano Lett.*, 2010, **10**, 4559.

313 D. S. Seferos, D. A. Giljohann, H. D. Hill, A. E. Prigodich and C. A. Mirkin, *J. Am. Chem. Soc.*, 2007, **129**, 15477.

314 A. Foubert, N. V. Beloglazova, A. Rajkovic, B. Sas, A. Madder, I. Y. Goryacheva and S. De Saeger, *TRAC*, 2016, **83**, 31.

315 A. Gole and C. J. Murphy, *Langmuir*, 2008, **24**, 266.

316 R. Bilan, F. Fleury, I. Nabiev and A. Sukhanova, *Bioconjugate Chem.*, 2015, **26**, 609.

317 K. Kang, C. Kan, A. Yeung and D. Liu, *Mater. Sci. Eng., C*, 2006, **26**, 664.

318 N. V. Beloglazova, A. Foubert, A. Gordienko, M. D. Tessier, T. Aubert, E. Drijvers, I. Goryacheva, Z. Hens and S. De Saeger, *Talanta*, 2016, **160**, 66.

319 O. Klykov and M. G. Weller, *Anal. Methods*, 2015, 7, 6443.

320 N. Abello, H. A. M. Kerstjens, D. S. Postma and R. Bischoff, *J. Proteome Res.*, 2007, **6**, 4770.

321 D. R. Dempsey, H. Jiang, J. H. Kalin, Z. Chen and P. A. Cole, *J. Am. Chem. Soc.*, 2018, **140**, 9374.

322 P. Cuatrecasas and I. Parikh, *Biochemistry*, 1972, **11**, 2291.

323 A. J. Lomant and G. Fairbanks, *J. Mol. Biol.*, 1976, **104**, 243.

324 D. Kahne and W. C. Still, *J. Am. Chem. Soc.*, 1988, **110**, 7529.

325 O. Koniev and A. Wagner, *Chem. Soc. Rev.*, 2015, **44**, 5495.

326 P. Ochtrop and C. P. R. Hackenberger, *Curr. Opin. Chem. Biol.*, 2020, **58**, 28.

327 N. Venkatesan and B. H. Kim, *Chem. Rev.*, 2006, **106**, 3712.

328 M. Amblard, J.-A. Fehrentz, J. Martinez and G. Subra, *Mol. Biotechnol.*, 2006, **33**, 239.

329 B. L. Oliveira, Z. Guo and G. J. L. Bernardes, *Chem. Soc. Rev.*, 2017, **46**, 4895.

330 T. Machida and N. Winssinger, *ChemBioChem*, 2016, **17**, 811.

331 C. W. Tornøe, C. Christensen and M. Meldal, *J. Org. Chem.*, 2002, **67**, 3057.

332 B. Cao, Y. Zheng, T. Xi, C. Zhang, W. Song, K. Burugapalli, H. Yang and Y. Ma, *Biomed. Microdevices*, 2012, **14**, 709.

333 D. C. Kennedy, C. S. McKay, M. C. B. Legault, D. C. Danielson, J. A. Blake, A. F. Pegoraro, A. Stolow, Z. Mester and J. P. Pezacki, *J. Am. Chem. Soc.*, 2011, **133**, 17993.

334 V. Bevilacqua, M. King, M. Chaumontet, M. Nothisen, S. Gabillet, D. Buisson, C. Puente, A. Wagner and F. Taran, *Angew. Chem., Int. Ed.*, 2014, **53**, 5872.

335 J. Dommerholt, F. P. J. T. Rutjes and F. L. van Delft, *Top. Curr. Chem.*, 2016, **374**, 16.

336 B. D. Fairbanks, E. A. Sims, K. S. Anseth and C. N. Bowman, *Macromolecules*, 2010, **43**, 4113.

337 B. L. Oliveira, Z. Guo, O. Boutureira, A. Guerreiro, G. Jiménez-Osés and G. J. L. Bernardes, *Angew. Chem., Int. Ed.*, 2016, **55**, 14683.

338 I. Nikić, T. Plass, O. Schraidt, J. Szymański, J. A. G. Briggs, C. Schultz and E. A. Lemke, *Angew. Chem., Int. Ed.*, 2014, **53**, 2245.

339 Z. Liu, F. Gan, N. Dong, B. Zhang, J. Wang and Y. Chen, *J. Mater. Chem. C*, 2019, **7**, 10789.

340 D. O. Li, M. S. Gilliam, X. S. Chu, A. Yousaf, Y. Guo, A. A. Green and Q. H. Wang, *Mol. Syst. Des. Eng.*, 2019, **4**, 962.

341 I. Murphy, P. Rice, M. Monahan, L. Zasada, E. Miller, S. Raugei and B. Cossairt, 2021, DOI: 10.33774/chemrxiv-2021-3p4pp.

342 N. H. Mohd, N. F. H. Ismail, J. I. Zahari, W. F. B. Wan Fathilah, H. Kargarzadeh, S. Ramli, I. Ahmad, M. A. Yarmo and R. Othaman, *J. Nanomater.*, 2016, **2016**, 4804271.

343 H. Yu, Y. Lu, Z. Feng, Y. Wu, Z. Liu, P. Xia, J. Qian, Y. Chen, L. Liu, K. Cao, S. Chen and W. Huang, *Nanoscale*, 2019, **11**, 9103.

344 X. Lu, Z. Zhang, Q. Xia, M. Hou, C. Yan, Z. Chen, Y. Xu and R. Liu, *Mater. Sci. Eng., C*, 2018, **82**, 190.

345 S.-H. Yang, *Appl. Phys. Lett.*, 2020, **116**, 120502.

346 R. Naaman, Y. Paltiel and D. H. Waldeck, *Nat. Rev. Chem.*, 2019, **3**, 250.